

Sediment provenance of the Lulehe Formation in the Qaidam basin: Insight to initial Cenozoic deposition and deformation in northern Tibetan plateau

Xing Jian¹ | Ling Fu² | Ping Wang^{3,4} | Ping Guan⁵ | Wei Zhang¹ | Hanjing Fu¹ | Haowei Mei¹

¹State Key Laboratory of Marine Environmental Science, College of Ocean and Earth Sciences, Xiamen University, Xiamen, PR China

²Research Institute of Petroleum Exploration and Development (RIPED), PetroChina, Beijing, PR China

³School of Geographical Science, Nanjing Normal University, Nanjing, PR China

⁴Jiangsu Center for Collaborative Innovation in Geographical Information Resource Development and Application, Nanjing, PR China

⁵MOE Key Laboratory of Orogenic Belts and Crustal Evolution, School of Earth and Space Sciences, Peking University, Beijing, PR China

Correspondence

Xing Jian, State Key Laboratory of Marine Environmental Science, College of Ocean and Earth Sciences, Xiamen University, Xiamen 361102, PR China.
Email: xjian@xmu.edu.cn

Funding information

Xiamen University Fundamental Research Funds for the Central Universities, Grant/Award Number: 20720190103 and 20720190097; National Natural Science Foundation of China, Grant/Award Number: 41806052 and 41902126

Abstract

Unravelling early Cenozoic basin development in northern Tibetan Plateau remains crucial to understanding continental deformation mechanisms and to assessing models of plateau growth. We target coarse-grained red beds from the Cenozoic basal Lulehe Formation in the Qaidam basin by combining conglomerate clast compositions, paleocurrent determinations, sandstone petrography, heavy mineral analysis and detrital zircon U–Pb geochronology to characterize sediment provenance and the relationship between deformation and deposition. The red beds are dominated by matrix-supported, poorly sorted clastic rocks, implying low compositional and textural maturity and short transport distances. Although most sandstones have high (meta)sedimentary lithic fragment contents and abundant heavy minerals of metamorphic origin (e.g., garnet, epidote and chlorite), spatiotemporal differences in detrital compositions are evident. Detrital zircon grains mainly have Phanerozoic ages (210–280 Ma and 390–480 Ma), but Proterozoic ages (750–1000 Ma, 1700–2000 Ma and 2300–2500 Ma) are also prominent in some samples. Analysed strata display dissimilar (including south-, north- and west-directed) paleocurrent orientations. These results demonstrate that the Cenozoic basal deposits were derived from localized, spatially diverse sources with small drainage networks. We advocate that initial sedimentary filling in the northern Qaidam basin was fed by parent-rocks from the North Qaidam–South Qilian belts and the pre-Cenozoic basement within the Qaidam terrane interior, rather than southern distant Eastern Kunlun regions. Seismic and drilling well stratigraphic data indicate the presence of paleohighs and syn-sedimentary reverse faults and noteworthy diversity in sediment thickness of the Lulehe Formation, revealing that the Qaidam terrane exhibited as several isolated depocenters, rather than a coherent basin, in the early stage of the Cenozoic deposition. We suggest the Cenozoic Qaidam basin to have developed in a contractional deformation regime, which supports models with synchronous deformation throughout most of Tibet shortly after the India–Eurasia collision.

KEYWORDS

basin analysis, detrital zircon geochronology, India-Eurasia collision, provenance analysis, Tibetan Plateau

1 | INTRODUCTION

The Tibetan Plateau is characterized by extremely high elevation (ca. 5 km above sea level), exceptional crustal thickness (ca. 70 km) and wide lateral extent (ca. 3 million km²) and is usually referred to as the “roof of the world”. This uniqueness makes it a popular testing ground for ideas concerning large-scale continental deformation, effect of large orogens on climate and interactions between the two (e.g., Clark, 2012; Miao et al., 2012; Molnar et al., 2010; Raymo & Ruddiman, 1992). How the plateau deformed and grew remains an outstanding issue and it remains controversial that northward propagating or synchronous, continuous deformation dominated the plateau uplift process (e.g., Clark, 2012; Molnar et al., 1993; Tapponnier et al., 2001; Wang, Zhao, et al., 2008; Zhang et al., 2004). The Tibetan Plateau is currently demarcated by the Longmenshan thrust belt to the east, the Western Kunlun and Qilian orogens to the north and the Himalaya orogen to the south (Figure 1a). The India-Eurasia collision in the early Cenozoic (50–55 Ma) created the south boundary of the plateau (Najman et al., 2010; van Hinsbergen et al., 2012). Although the collision was probably not the only driving force for Tibetan crust deformation and pre-collisional crustal thickening and high-relief existed in the southern and central Tibet regions (Kapp et al., 2005, 2007; Murphy et al., 1997; Rohrmann et al., 2012; Volkmer et al., 2007; Wang, Zhao, et al., 2008), continuous convergence between the India and Eurasia plates since the collision has played a crucial role in forming the current framework and high topography of the plateau (Molnar & Stock, 2009; Wang et al., 2014; Yin & Harrison, 2000; Yuan et al., 2013 and references therein). In this case, response of the northern Tibet (ca. 1500–2000 km away from the collisional zone) to the collision is pivotal to understanding the deformation and uplift mechanism of the plateau. However, controversies about the northern Tibet crustal thickening process have persisted. Proposed hypotheses mainly include (1) crustal shortening along the north boundary of the plateau at the onset of collision, followed by shortening of the remainder of northern Tibet at a later time (Dayem et al., 2009; Kong et al., 1997); (2) northward propagating shortening within the northern Tibet (Wang, Zhao, et al., 2008; Wang et al., 2017) and (3) synchronous distributed crustal shortening soon after collision (Clark, 2012; Clark et al., 2010).

Highlights

1. The Cenozoic Lulehe Formation in the Qaidam basin is featured by matrix-supported, poorly-sorted red beds.
2. The red beds were derived from localized, diverse sources with small drainage networks.
3. Isolated depocenters occurred when Cenozoic deposition initiated, under a contractional deformation regime.
4. The findings support models with synchronous deformation throughout most of Tibet shortly after the India-Eurasia collision.

These different crustal deformation patterns expect to contribute to distinct earth-surface processes (e.g., weathering, erosion, sediment transport, deposition and basin development) in northern Tibet regions during the Cenozoic. The Qaidam basin, as the largest intracontinental sedimentary basin in northern Tibet (Figure 1b), contains voluminous Cenozoic siliciclastic rocks sourced from the surrounding high-elevation mountains (e.g., Bao et al., 2017; Bush et al., 2016; Cheng, Fu, et al., 2016; Cheng, Garzzone, Mitra, et al., 2019; Du et al., 2018; Hong et al., 2020; Jian, Guan, Zhang, & Feng, 2013; Jian, Guan, Zhang, Zhang, et al., 2013; Lu et al., 2018; Nie et al., 2020; Song et al., 2019; Wang et al., 2017; Zhuang et al., 2011). The Cenozoic sedimentary succession commonly unconformably lies on Jurassic–Early Cretaceous sedimentary strata or contacts with pre-Cenozoic crystalline basement and begins with coarse-grained red beds (Figures 2–5, named as the Lulehe Formation) in most places (Guan & Jian, 2013; Jian, Zhang, et al., 2019; Zhuang et al., 2011). Sediment provenance and depositional process of these coarse-grained red beds (Figure 3) are a key to better understand the response of Cenozoic basin development to northern Tibetan crustal deformation.

Previous provenance analyses on the Lulehe Formation have generated different interpretations. Deposits from the Dahonggou (DHG) section (Figure 1c, one of the best Cenozoic outcrops) are interpreted to be initially derived from the southern distant Qimantagh and Eastern Kunlun Ranges based on detrital zircon geochronological results (abundant Permian–Triassic detrital zircon U–Pb ages, Bush et al., 2016; Nie et al., 2020; Wang et al., 2017).

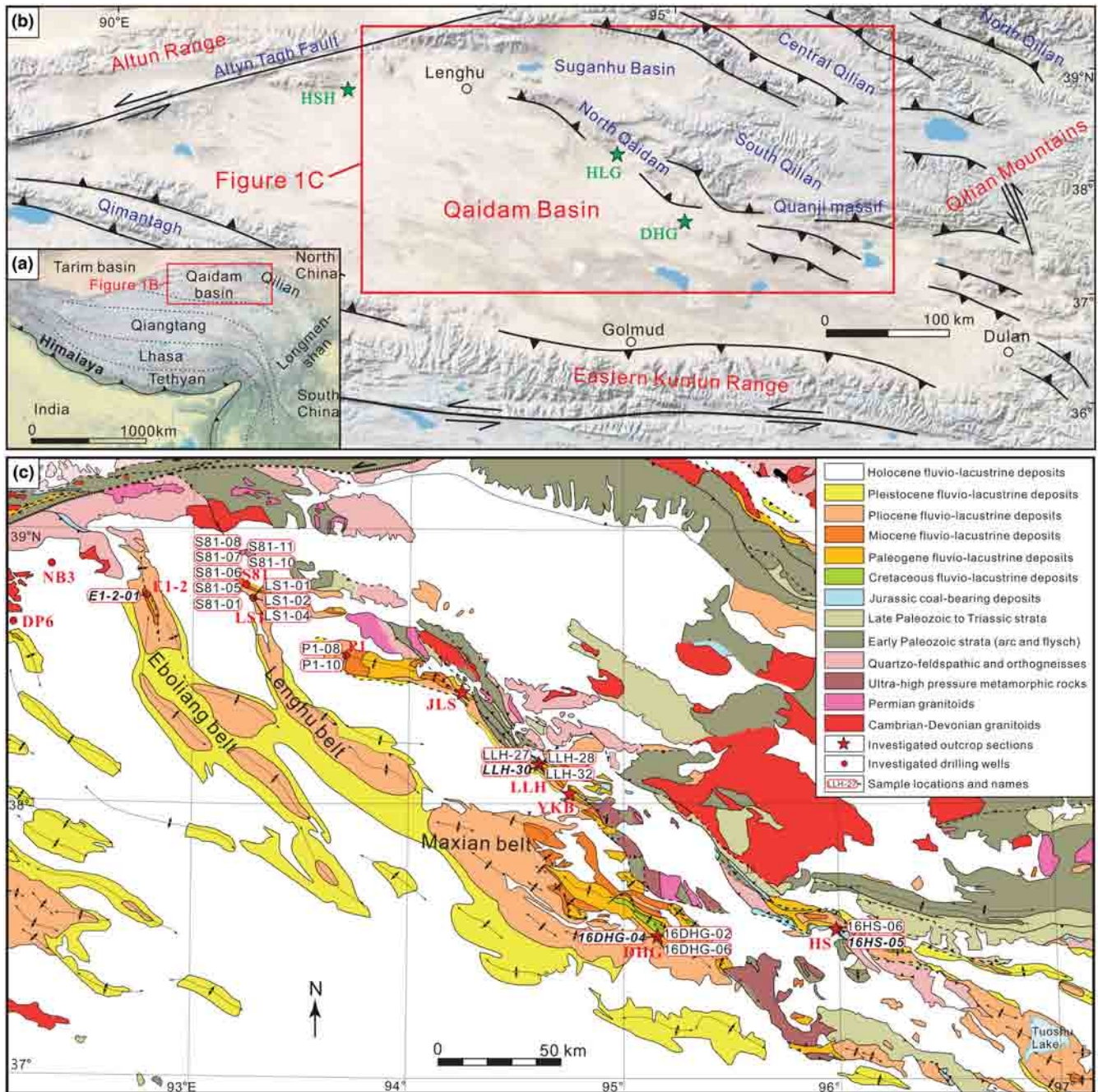


FIGURE 1 (a) Major tectonic elements of the Tibetan plateau and its surrounding regions. (b) Tectonic settings of the Qaidam basin, modified from Zuza et al. (2016); Yu, Guo, et al. (2017) and Jian et al. (2018). The green pentagram symbols indicate the locations of reported Paleogene sections for magnetostratigraphy study (HSH: Hongsanhan section, from Sun et al. (2005); HLG: Hongliugou section, from Fang, Galy, et al. (2019); DHG: Dahonggou section, from Ji et al. (2017), Wang et al. (2017) and Nie et al. [2020]). (c) Geological map of the northern Qaidam basin and the south Qilian-north Qaidam metamorphic belts (modified from Yin, Dang, Wang, et al. [2008]) and locations of the investigated Lulehe Formation outcrop sections (JLS: Jielsu section; LLH: Lulehe section; YKB: Yukabei section; HS: Hongshan section), drilling wells and samples (bold italic symbols indicate detrital zircon dating samples) in this study.

In contrast, these coarse-grained siliciclastic deposits are interpreted to be fed by nearby sources to the north, that is, the North Qaidam and South Qilian thrust belts (Lu et al., 2018; Song et al., 2019; Zhuang et al., 2011). The Lulehe Formation deposits in northwest regions of the Qaidam basin have different detrital zircon U–Pb

age populations (dominated by early Palaeozoic and Neoproterozoic ages, Cheng, Garziona, Mitra, et al., 2019; Cheng, Jolivet, et al., 2016) from those at the DHG section. Uplift and erosion of the Altun Range and the west parts of the South Qilian belt are considered to initiate the Cenozoic sedimentation and to provide detritus for the

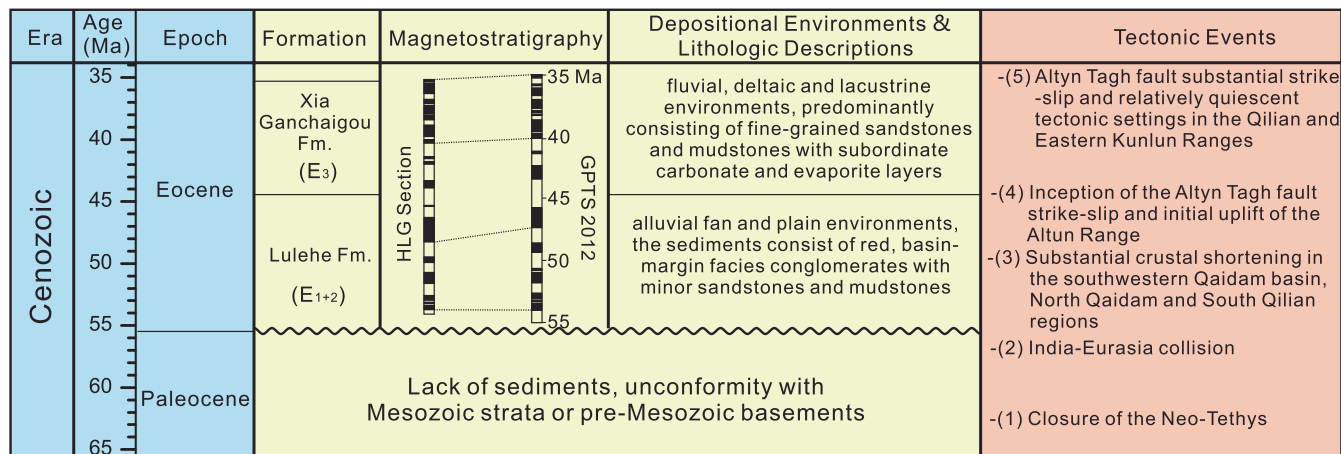


FIGURE 2 Early Cenozoic stratigraphy, formations, lithologic descriptions of the northern Qaidam basin and major tectonic events. The magnetostratigraphic column of the HLG section (see Figure 1b for its location) and the correlation with the reference geomagnetic polarity time scale (GPTS 2012) are modified from Fang, Galy, et al. (2019).

northwest regions (Cheng, Garzzone, Mitra, et al., 2019; Cheng, Jolivet, et al., 2016). These diverse provenance interpretations reveal that large-scale tectonic explanations based on analysis data from only one sedimentary section or a local region may be biased. Therefore, a multi-method, multi-dimensional, basin-wide investigation is essential to unravel sediment provenance and depositional process of those coarse-grained red beds.

We target the Lulehe Formation deposits from several outcrop sections and drilling wells in the Qaidam basin (Figure 1c). We combine field-based paleocurrent orientation, conglomerate clast composition, sandstone petrography, heavy mineral and detrital zircon U–Pb geochronological data to conduct an integrated provenance analysis for the Lulehe Formation strata. The objective of this study is to reconstruct provenance and depositional process of the Cenozoic basal coarse-grained sediments and to better understand how the basin development and surface processes in northern Tibet responded to the India-Eurasia collision.

2 | GEOLOGICAL SETTING

2.1 | Background of the Qaidam basin

The Qaidam basin covers ca. 120,000 km² and is situated about 2.7–3.0 km above sea level. It is bounded by three large mountain ranges (i.e., the Qilian, Altun and Eastern Kunlun Ranges) that reach elevations of up to 5 km. The Qaidam basin has experienced a complex climatic history since the Cenozoic (Jian et al., 2014; Sun et al., 2020) and the current basin, as a part of the arid Central Asia, has extremely dry and cold climates due to such topographic settings, long distances away from oceans and

the dominant westerly atmospheric circulations (Chen et al., 2010; Molnar et al., 1993). Due to the convergence between the India and Eurasia plates and the contractional settings, a series of thrust fold belts with NW–SE direction are present inside the Qaidam basin (Figure 1c) and reverse faults are developed along the north and south margins (Figure 5). Furthermore, the Qaidam basin is an important petroliferous basin for hydrocarbon production in northwest China (Zhang et al., 2018 and reference therein). A great number of wells have been drilled by the Qinghai Oilfield Company, PetroChina since 1950s. The on-going hydrocarbon exploration has obtained high-quality seismic data and valuable drilling rock cores and thus allows for a comprehensive study on the subsurface strata of the basin.

2.2 | Cenozoic stratigraphic framework and sedimentary environments of the Qaidam basin

The Cenozoic sedimentary succession of the Qaidam basin is exceptionally thick (>10 km in the basin centre) and is commonly divided into seven stratigraphic units (Figures 2a and 5) as follows: (1) Lulehe Formation (E₁₊₂, Figure 2); (2) Xia Ganchaigou Formation (E₃, divided into E₃¹ and E₃² for local hydrocarbon exploration and development); (3) Shang Ganchaigou Formation (N₁); (4) Xia Youshashan Formation (N₂¹); (5) Shang Youshashan Formation (N₂²); (6) Shizigou Formation (N₂³) and (7) Qigequan Formation (Q₁₊₂).

Previous investigations demonstrate that sedimentary depocenters shifted east-ward in the Qaidam basin during the Cenozoic (Bao et al., 2017; Yin, Dang, Zhang, et al., 2008). As a result, the Cenozoic strata display highly

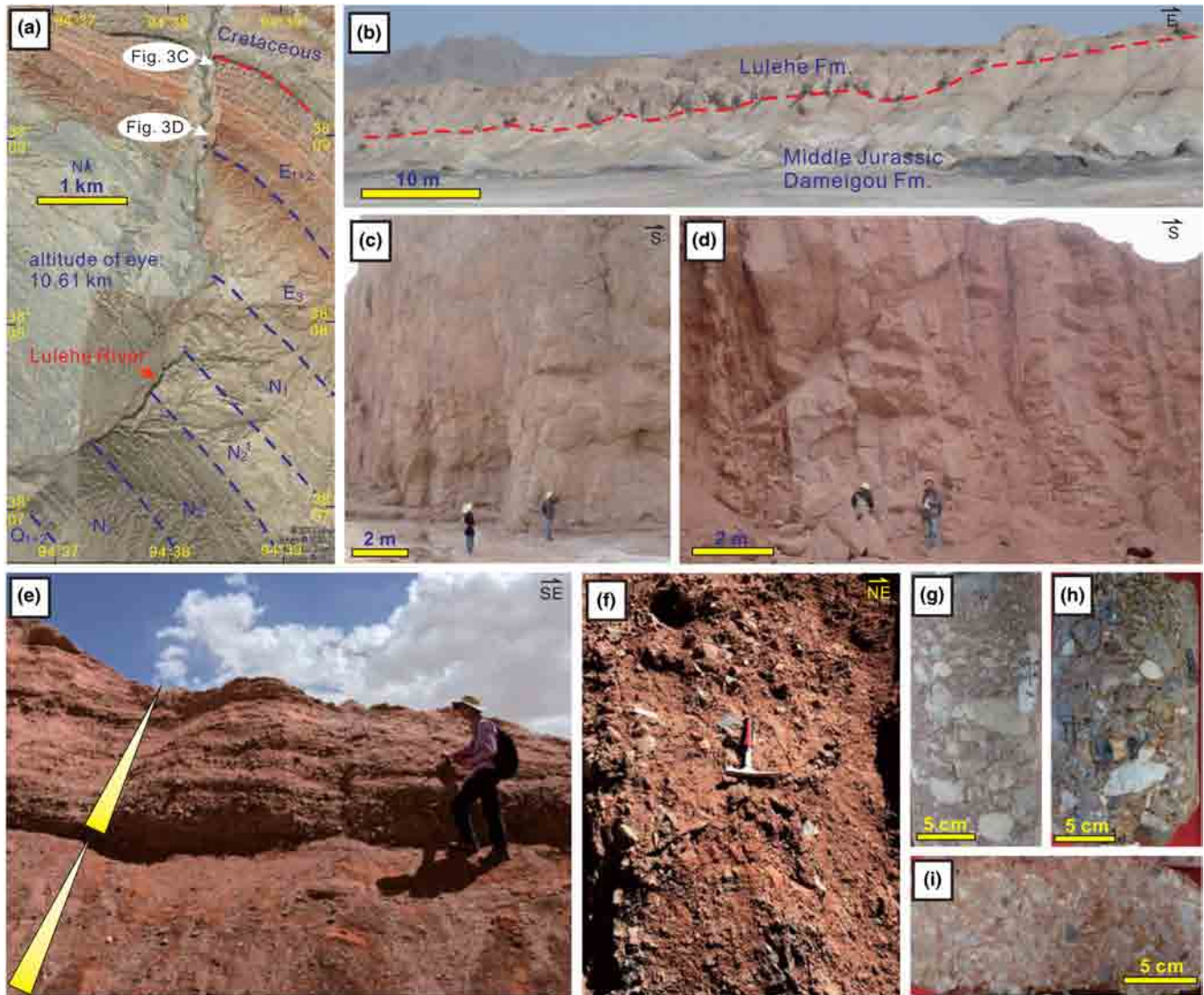


FIGURE 3 Representative features of the Lulehe Formation outcrops and borehole rock cores in the Qaidam basin. (a) a Google earth image (www.earth.google.com) showing Cenozoic sedimentary outcrops of the LLH section. (b) the Lulehe Formation strata unconformably contact with the underlying middle Jurassic Dameigou formation strata to the north of the LLH section; (c) red, thick and massive conglomerates in lower parts of the Lulehe Formation (LLH section); (d) red, interbedded sandstone and mudstone sequences in upper parts of the Lulehe Formation (LLH section); (e) upward-fining conglomerate red bed sequences at the DHG section; (f) poorly sorted, matrix-supported conglomerate red beds at the JLS section; (g) poorly sorted conglomerates from the well DP6; (h) poorly sorted conglomerates from the well NB3; (i) carbonate clast-rich conglomerates from the well S81. For locations of the outcrop sections and drilling wells, see [Figure 1c](#).

spatial and stratigraphic variations in lithology. The western Qaidam basin is characterized by mixed carbonate-siliciclastic deposits with minor evaporite layers (Jian et al., 2014 and references therein; Guo et al., 2017; Zhang et al., 2018), whereas the Cenozoic strata in the northern and eastern Qaidam basin are dominated by siliciclastic deposits (Cheng et al., 2021; Fu et al., 2022; Jian, Guan, Zhang, & Feng, 2013; Jian, Guan, Zhang, Zhang, et al., 2013). Vertically, the Cenozoic strata generally indicate a stacking pattern of coarse-grained red bed deposits in the bottom (E_{1+2}), followed by fine-grained-dominated deposits (E_3 , N_1 and N_2^1) and then coarse-grained deposits

in upper units (N_2^2 , N_2^3 and Q_{1+2}) for most regions (Guan & Jian, 2013; Jian, Guan, Zhang, Zhang, et al., 2013; Jian et al., 2014; Zhuang et al., 2011).

The Lulehe Formation strata are widely distributed in the northern Qaidam basin and are characterized by red, massive, thick-bedded conglomerates ([Figure 3](#)) with subordinate sandstones ([Figure 4](#)). These deposits are generally regarded as a product of high-gradient depositional systems (i.e., basin-margin facies) (Guan & Jian, 2013; Zhuang et al., 2011). The overlying E_3 , N_1 and N_2^1 fine-grained-dominated deposits are interpreted to form in fluvial, deltaic and lacustrine environments

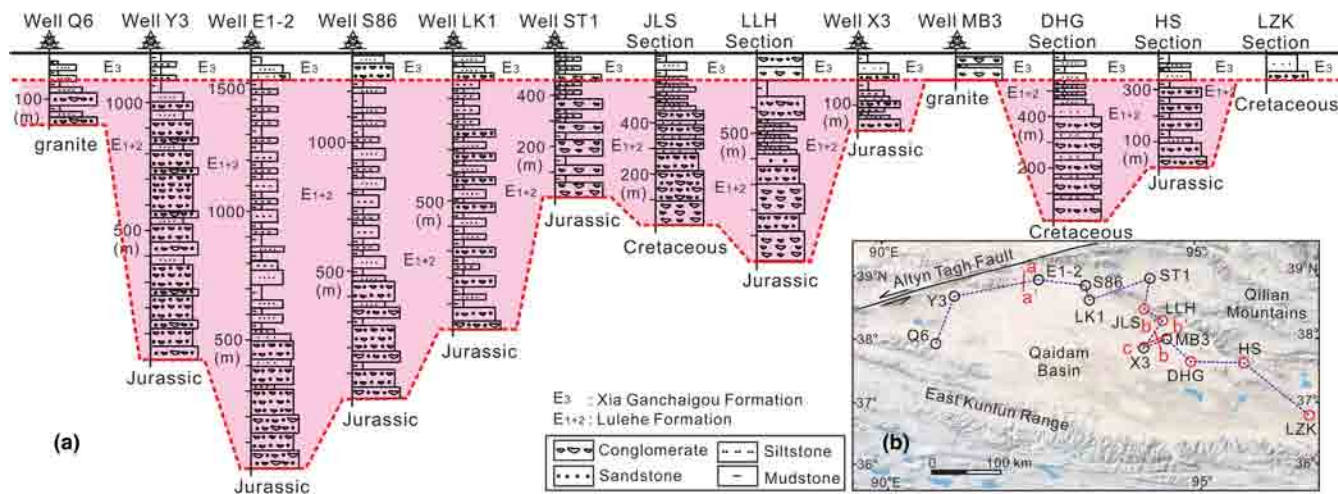


FIGURE 4 Stratigraphic correlations of the Lulehe Formation strata across the Qaidam basin. The drilling well data are from Guan and Jian (2013). Although most Lulehe Formation deposits are dominated by conglomerate red-beds, with subordinate sandstone layers, these strata display strong spatial diversity in thickness (0–1500 m). Note that the pre-Cenozoic basement granites are overlain by the middle–late Eocene Xia Ganchaigou formation strata in the Maxian paleohigh region (e.g., well MB3), without Lulehe Formation strata. And several pre-Cenozoic basement granite samples were dated to have Permian ages (e.g., 271 ± 2 Ma and 291 ± 2 Ma) (Cheng et al., 2017).

(Guan & Jian, 2013; Jian et al., 2018; Zhuang et al., 2011) and a relatively unified megalake is inferred to have existed during the Oligocene–Miocene (Liang et al., 2021; Wu et al., 2021). Contraction of the huge Qaidam paleomagelake is evidenced by the widespread N_2^3 and Q_{1+2} coarse-grained deposits (Fu et al., 2022; Guan & Jian, 2013; Yu et al., 2021) and dozens of small scattered saline and brackish lakes are currently present in the Qaidam basin.

2.3 | Depositional age of the Lulehe formation

There are two distinct viewpoints on the depositional age of Lulehe Formation strata in the Qaidam basin. A traditional viewpoint is that the Cenozoic sedimentation started in the early Eocene and the Lulehe Formation was deposited ca. 43.5–54 Ma, based on magnetostratigraphy and palaeontology studies from several outcrop sections (Fang, Galy, et al., 2019; Ji et al., 2017; Sun et al., 2005; Figure 2). A new age model supports late Oligocene–early Miocene initial deposition (ca. 20–25 Ma) of the Cenozoic strata, based on magnetostratigraphic and paleontological constraints on the DHG section in the northeastern Qaidam basin (Nie et al., 2020; Wang et al., 2017).

A detailed review and comparison analysis of these two age models was recently reported by Cheng et al. (2021), in which the traditional viewpoint of an early Eocene onset of sediment accumulation in the Qaidam basin was preferred. An Eocene age, is supported by age controls from mammal fossils, sporo-pollen compositions, thermochronological data as well as regional lithostratigraphic

correlations (Cheng et al., 2021 and references therein). The Xia Ganchaigou Formation strata from an outcrop section (i.e., the HSH section, see Figure 1b for its location) in the northwestern Qaidam basin were previously assigned as upper Eocene, based on magnetostratigraphic correlations and Ostracoda fossil assemblages (Sun et al., 2005). This implies that the underlying Lulehe Formation was most likely deposited prior to the late Eocene. Recently published oxygen isotopic data of sedimentary carbonates and carbon isotopic data of long-chain n-alkanes from the DHG section demonstrate that, in the case of Eocene-onset for the Lulehe Formation deposition, stable isotope-recorded regional moisture fluctuations can correspond well with global climatic conditions (Sun et al., 2020). Widespread evaporite rocks in the Xia Ganchaigou Formation strata from the western Qaidam basin (Guo et al., 2017), which can be well correlated with similar deposits in the adjacent Eocene sedimentary basins (such as the Xining basin [Fang, Fang, et al., 2019; Meijer et al., 2019] to the east, constrained by tuff radiometric ages) and in the whole Eocene subtropical hot-dry zone in East Asia (Guo et al., 2008), support the initiation of sediment accumulation prior to ca. 50 Ma in the Qaidam basin. Low-temperature thermochronology data demonstrate widespread Eocene exhumation in the surrounding Qilian, Eastern Kunlun and Altun Ranges (An et al., 2020; Jian et al., 2018; Li, Zusa, et al., 2020 and references therein), which could result in deposition of the mountain materials in the adjacent sedimentary basins. Furthermore, available interbedded volcanic rocks and tuff rocks from several Cenozoic nonmarine basins in the northern and eastern Tibetan Plateau were dated

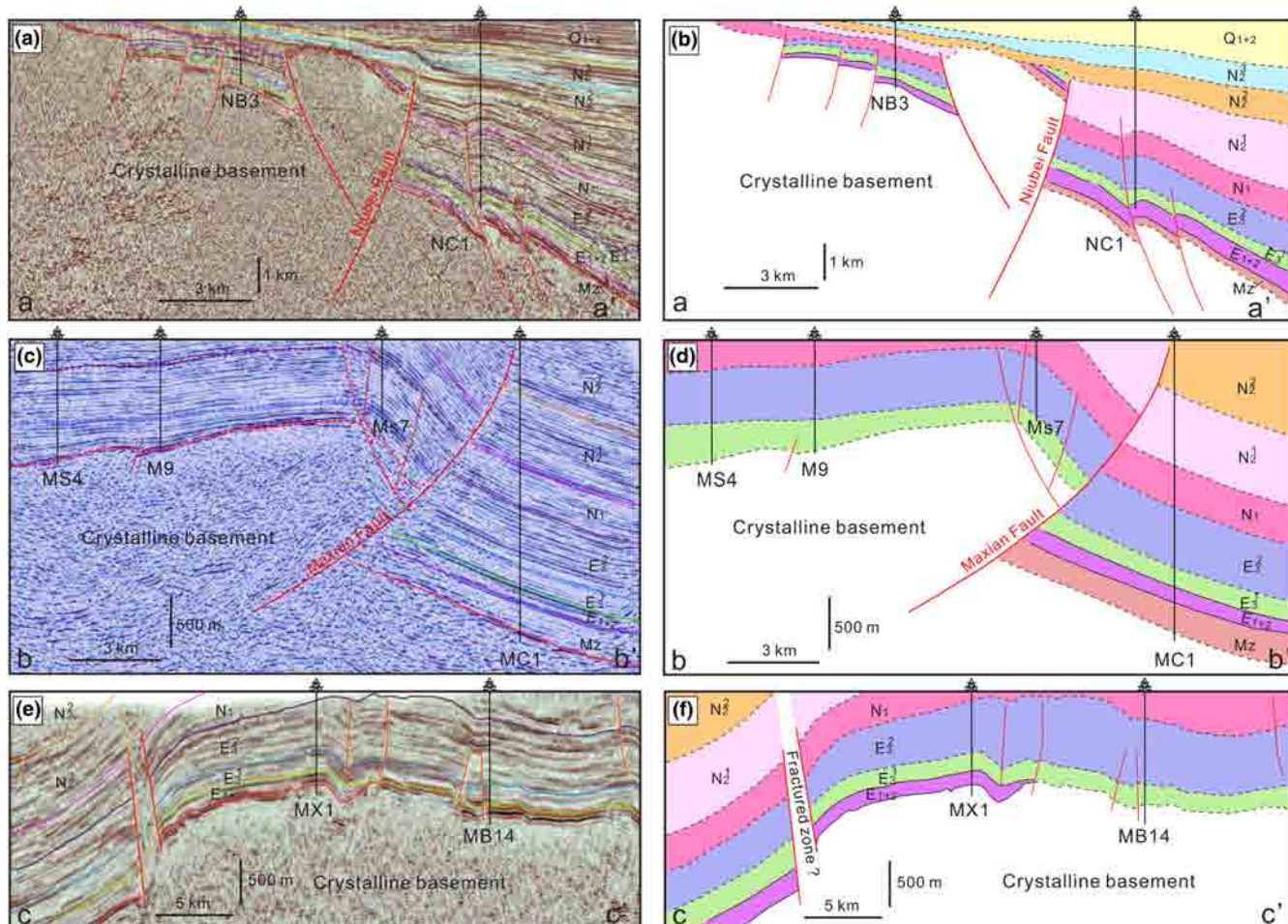


FIGURE 5 Representative 3D seismic profiles in the northern Qaidam basin. (a) and (b): A profile close to the Altun range showing growth strata for the Lulehe Formation. The Lulehe Formation is featured by thick deposits in the footwall of the Niubei fault and comparatively thin deposits in the hanging wall of the fault. (c) and (d): A profile across the Maxian fault, close to the Qilian Mountains. The Lulehe Formation strata therein are present in the footwall but absent in the hanging wall. (e) and (f): A profile in the Maxian paleohigh (modified from Jian, Zhang, et al. [2019]). The Lulehe Formation shows a clear eastward stratigraphic onlap. These images indicate that the Qaidam terrane was most likely under highland-erosion and lowland-deposition conditions at the beginning of the Cenozoic deposition and the Niubei and Maxian faults were active during the Lulehe Formation deposition. The seismic data were collected from the Qinghai oilfield company, PetroChina. Mz: Mesozoic; E₁₊₂: Lulehe Formation; E₃: Xia Ganchaigou formation; N₁: Shang Ganchaigou formation; N₂¹: Xia Youshashan formation; N₂²: Shang Youshashan formation; N₂³: Shizigou formation; Q₁₊₂: Qigequan formation. For locations of these seismic profiles, see Figure 4b.

as 43–52 Ma (Horton et al., 2002; Meijer et al., 2019; Tang et al., 2017), revealing that sediment accumulation occurred in numerous areas of the plateau during the Eocene.

2.4 | Description of potential detrital sources for the Cenozoic Qaidam basin

It is well known that the three high-relief, huge mountains around the Qaidam basin have different geological history and bedrock lithology (e.g., Wu et al., 2016; Zhang et al., 2021; Zusa et al., 2018). The Qilian Mountains are to the northeast as a ca. 300 km-wide, 1000 km-long,

metamorphic rock-rich fold-thrust belt (Gehrels et al., 2003a; Zusa et al., 2018) and forms the northern boundary of the Tibetan Plateau. From north to south, the Qilian Mountains consist of the North Qilian early Palaeozoic complex, the Central Qilian Proterozoic basement and the South Qilian-North Qaidam metamorphic belt (Figure 1b). The Qilian Mountains are dominated by Proterozoic–early Palaeozoic metamorphic rocks, Proterozoic–Mesozoic marine (meta)sedimentary strata and early Palaeozoic igneous rocks (Gehrels et al., 2003b). These rocks are regarded as records of a complete tectonic evolutionary history from continental breakup to ocean basin evolution (the Proto-Tethys and Qilian oceans), and to the ultimate collision of related micro-continent during

the early Palaeozoic to Devonian (400–520 Ma) (Zhang et al., 2021; Zuza et al., 2018 and references therein). However, the Eastern Kunlun Range, as a ca. 1000 km-long, latitudinally trending, granitoid-rich orogenic belt, is mainly composed of Cambrian–Early Devonian (400–500 Ma) and Permian to Triassic (220–290 Ma) granitoid rocks (Figure 6), Neoproterozoic basement rocks and subordinate sedimentary rocks (Cheng et al., 2017; He et al., 2018; Jian, Weislogel, et al., 2020 and references therein). The Eastern Kunlun orogenic belt is thought to document successive subduction-closure of the Proto-Tethys and Paleo-Tethys Oceans and related continent amalgamation during the Palaeozoic to early Mesozoic (Jian, Weislogel, et al., 2019, 2020; Li et al., 2013; Wu et al., 2016). Therefore, Phanerozoic zircon age signatures of the Eastern Kunlun Range are featured by 220–290 Ma and 400–500 Ma age populations, whereas most areas in the Qilian Mountains (e.g., the Central and North Qilian belts) display dominant 400–520 Ma zircon age signatures (Figure 6b; Table S1 in the Supporting Information).

Different from the Eastern Kunlun and Qilian Mountains, the Altun Range is considered to be unrelated to any individual paleo-ocean evolution and

tectono-magmatic history. Instead, the formation, deformation and uplift of the Altun Range is closely related to activities of the left-lateral strike-slip Altyn Tagh Fault (Wu, Lin, et al., 2019). Given the ca. 375 km left-lateral offset, the north part of the Altyn Tagh Fault is composed of rocks that are similar to those in the Qilian Mountains (Gehrels et al., 2003b) and the pre-Mesozoic crystalline rocks therein mainly show early Palaeozoic ages, with subordinate Neoproterozoic and Paleoproterozoic ages (Figure 6; Cheng et al., 2017; Yu, Fu, et al., 2017 and references therein). In contrast, bedrocks exposed in the south part of the strike-slip fault are relatively rare and show different zircon age signatures (Permian, Silurian and Ordovician) from those in the north part. These bedrocks indicate the western Qaidam basin margin basement features. Although the crystalline basement within the basin is mostly covered by thick Mesozoic–Cenozoic sedimentary strata and remains comparatively poorly known, available borehole granitoid rocks from the basin interior indicate dominant Permian (260–290 Ma), Ordovician–Early Devonian (400–470 Ma) and minor Neoproterozoic (900–950) ages (Figure 6; Table S1). Similar geochemical compositions and U–Pb ages between these borehole

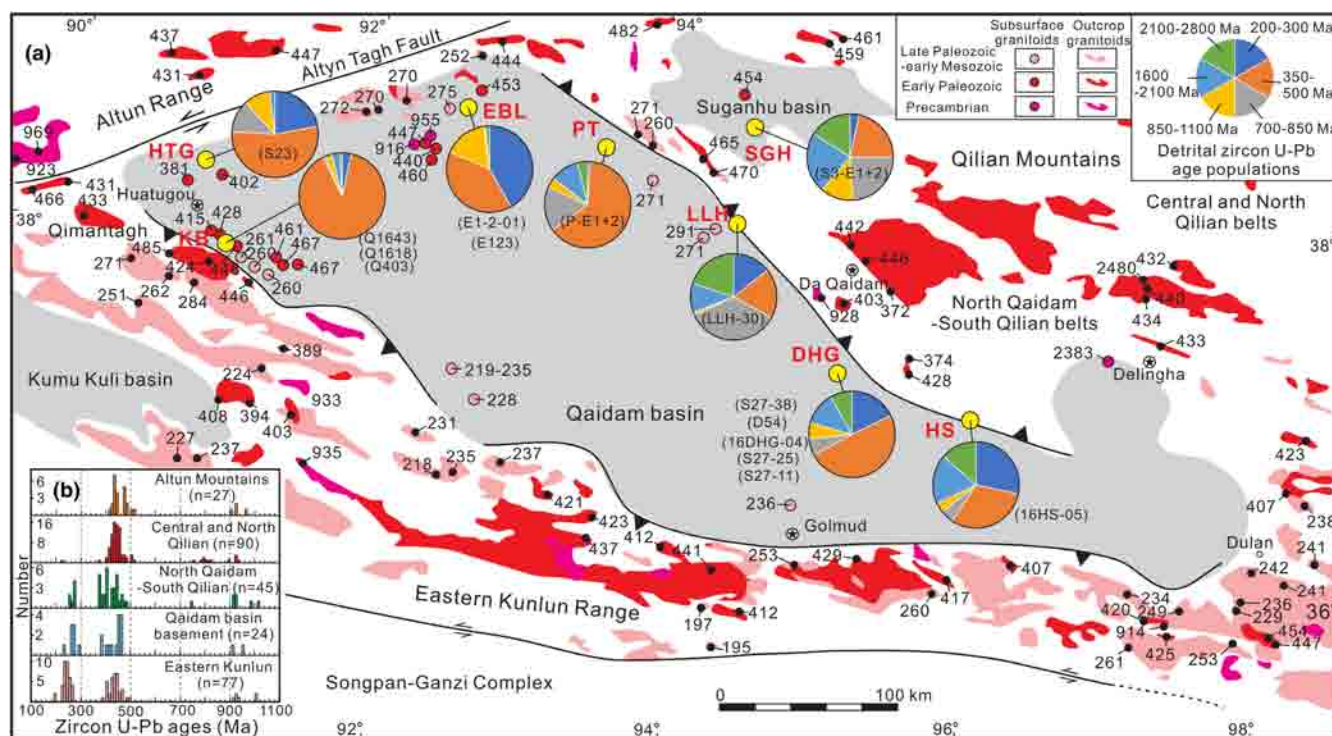


FIGURE 6 (a) Distributions and representative zircon U–pb ages of granitoid rocks in the northern Tibet, modified from Jian, Weislogel, et al. (2020). Pie charts indicate detrital zircon U–pb age populations of the Lulehe Formation strata (including published [Table S5] and new data [Table S4] in this study, see Figure S4 in the Supporting Information for the KDE plots of each sample). (b) Histograms indicate published granitoids zircon U–pb ages (Table S1) of the Qaidam basin crystalline basement and the surrounding mountains, modified from Jian, Weislogel, et al. (2020). Note that granitoids with Paleoproterozoic ages are also widely distributed in the north Qaidam-south Qilian belt (i.e., within the Qianji massif, Gong et al., 2012; Yu, Guo, et al., 2017; Yu et al., 2019), but those Paleoproterozoic ages are not involved in these histogram plots and age data of meta-granitoids in the northern Tibet are not included.

granitoids and the Eastern Kunlun granitoid rocks favour that the Qaidam basin regions had experienced similar tectono-magmatic episodes with the Eastern Kunlun Range (Cheng et al., 2017; Jian, Weislogel, et al., 2020). Therefore, the basement of the Qaidam basin is thought to be not mechanically stronger than its surrounding ranges and might pertain to a tectono-magmatic rejuvenated craton (Cheng et al., 2017), not as typical as the nearby rigid Tarim basin. More and more studies have realized that the northward Paleo-Tethys subduction did not only occur beneath the Kunlun-Qaidam terrane but also even influenced the regions of the North Qaidam and South Qilian metamorphic belts (Jian, Weislogel, et al., 2020; Wu et al., 2016; Zhang et al., 2021 and references therein). As a result, Permian arc-related granitoid rocks are also present in these two belts (Figure 6).

Precambrian history of the northern Tibet region is also well worth deep concern for the Qaidam basin sediment provenance interpretation, especially for detrital zircon provenance determination. The Kunlun, Qaidam and Qilian terranes are thought to be involved in late stage of the Grenvillian orogenesis and may correlate with the South China block before the Rodinia breakup (He et al., 2018; Jian, Weislogel, et al., 2020; Song et al., 2012; Yu et al., 2013) and thus Precambrian zircon age signatures of these terranes are characterized by early Neoproterozoic (800–1000 Ma) ages (Figure 6). Furthermore, the Quanji massif (Figure 1b; also named as Oulongbuluke block in some studies), as a part of the South Qilian-North Qaidam metamorphic belt (Figure 1b), was often underestimated in previous detrital zircon provenance studies. This massif is thought to have experienced several stages of tectono-magmatic events during the Paleoproterozoic and to have a possible affinity to the North China and Tarim blocks during the Precambrian (Chen et al., 2013; Gong et al., 2012; Yu, Fu, et al., 2017; Zhang et al., 2021). Detrital zircon geochronology results of the Quanji basement Precambrian metasedimentary rocks and Precambrian granitic rocks suggest characteristic zircon age signatures of 1800–2000 Ma and 2350–2500 Ma (Chen et al., 2013; Gong et al., 2012; Yu, Fu, et al., 2017). These two Paleoproterozoic age clusters are also indicated in detrital zircon U–Pb dating results of several modern river sand samples from this region (Zhang et al., 2021 and references therein).

3 | ANALYTICAL METHODS

Both outcrop sections and drilling well rock cores were investigated (Figure 1c). Sandstone samples were collected for petrography, heavy mineral analysis and detrital zircon U–Pb geochronology. Paleocurrent orientations

were mainly determined by pebble-cobble imbrications of the Lulehe Formation conglomerates and all the measurements were corrected for horizontal bedding rotations. These measuring locations include some sampled outcrops and other outcrops where such indicators were accessible. Conglomerate clast counts were collected to augment sediment provenance data and rock types of 50–100 clasts were counted using a 5-cm spacing over a 50-cm by 50-cm grid for outcrops and a 2-cm spacing over a 10-cm by 10-cm grid for drilling rock cores.

Fresh sandstone samples were prepared into 30 μm -thick standard thin sections for petrographic analysis. Model analysis of 18 selected samples was carried out using the Gazzi-Dickinson method under a polarizing microscope, with greater than 400 points counted per sample (Dickinson, 1985). A total of 16 sandstone samples were selected for heavy mineral analysis. The samples were preliminarily crushed and 63–250 μm fractions were sieved. Carbonate components and Fe-Mn oxide coatings were removed from the 63–250 μm fractions by soaking in 1 N acetic acid for 24 h under 60°C. Heavy minerals were then separated by heavy liquid tribromomethane (2.89 g/cm³) from the 63–250 μm fractions and subsequently weighted and mounted on glass slides with Canada balsam. More than 200 transparent heavy mineral grains were identified and point-counted at suitable regular spacing for each sample using a polarizing microscope (Jian, Zhang, et al., 2020).

Four sandstone samples were selected for detrital zircon U–Pb geochronological analysis. The selected sandstone samples (1–2 kg for each sample) were crushed (ca. 60 mesh), washed and then loaded with heavy liquids. Magnetic minerals were removed from the heavy fractions using a magnetic separator. All the visible zircon crystals (most >30 μm) were then separated from the heavy mineral fractions by hand-picking under a binocular microscope. The obtained grains were adhered to targets using epoxy resins and polished to section the crystals for imaging and dating. Laser-ablation-inductively coupled plasma-mass spectrometry (LA-ICP-MS) U–Pb analyses were performed at Peking University (sample E1-2-01, using an Agilent 7500a ICPMS equipped with a 193-nm laser) and Nanjing Normal University (samples LLH-30, 16DHG-04 and 16HS-05, using an Agilent 7500a ICP-MS equipped with a New Wave 213-nm laser). Detrital zircon grains with apparent inclusions or cracks were avoided and about 80–120 grains were selected randomly (regardless of the grain sizes) for each sample analysis, to avoid bias from detrital grain selection. Spot size was 32 μm in diameter for laser ablation; frequency was 10 Hz and Helium was applied as a carrier gas. The dating was monitored using standard-sample bracketing with the Plesovice

(337 Ma) and 91,500 (1062 Ma) zircon reference materials. Measured data were corrected to common Pb using the measured non-radiogenic ^{204}Pb (Andersen, 2002). U–Pb ages with poor precision ($>\pm 10\%$) and high discordance (the discordance between $^{206}\text{Pb}/^{238}\text{U}$ and $^{207}\text{Pb}/^{235}\text{U} > 15\%$ and reverse discordance $> 15\%$) were omitted from plotting and from interpretation. Ages < 1000 Ma are based on initial-Pb corrected $^{206}\text{Pb}/^{238}\text{U}$ ratios, whereas ages > 1000 Ma are based on initial-Pb corrected $^{206}\text{Pb}/^{207}\text{Pb}$ ratios.

4 | RESULTS

4.1 | Paleocurrent orientations

The Lulehe Formation strata display diverse paleocurrent orientations (Figure 7a). The HS and LLH sections show dominantly south- and southwest-directed paleoflow, whereas the paleocurrent orientations at the YKB and DHG sections generally trend toward the northwest (Figure 7a). The JLS section indicates mainly southwest-directed and subordinately northeast- and east-directed paleoflow. Furthermore, paleocurrent orientations of different stratigraphic layers of the Lulehe Formation strata from a single outcrop section are also dissimilar. For example, the lower Lulehe Formation at the DHG section shows northeast-directed paleoflow, whereas the upper Lulehe Formation therein has south-directed paleoflow (Figure 8).

4.2 | Conglomerate clast characteristics

The Lulehe Formation conglomerate beds are both clast-supported (Figure 3e,g,h) and matrix-supported (Figure 3f,i) and commonly exhibit massive bedding structures with rare cross beddings. Conglomerate clast sizes range from 2 to 50 cm, with an average size of ca. 5 cm. Clasts in the clast-supported conglomerate beds are typically subrounded to rounded and are moderately to well sorted, whereas clasts in the matrix-supported conglomerate beds are typically very angular to subangular and are relatively poorly sorted. The Lulehe Formation conglomerate clast compositions are diverse in different locations (Figure 7b) and in different layers of the same section (such as the DHG section, Figure 8). Identified clasts are dominated by sedimentary and metasedimentary rocks, including carbonate rocks, shales, sandstones, cherts, schists and quartzites (Figure 7b). Conglomerate strata from several locations (such as wells DP6 and NB3) are featured by carbonate rocks-dominated clasts. Igneous rock clasts (e.g., granites and diorites) are also largely

present in some conglomerate beds (e.g., Well NB3 and the JLS and LLH sections).

4.3 | Sandstone petrography

The Lulehe Formation sandstones have quite diverse textures and compositions (Figures 7c, 8 and 9). Samples from sandstone interlayers within massive conglomerate beds are typically matrix-supported and poorly sorted (Figure 9a,b), whereas samples from thick sandstone beds are grain-supported and moderately to poorly sorted (Figure 9c–e). Percentages of matrix and cements (mainly argillaceous and red Fe–Mn oxide-like materials) are greater than 50% in some counted samples (e.g., the samples from the DHG section, Figure 10a). Framework grains are angular to subangular (Figure 9a–e) and are mainly composed of quartz (31%–83%) and sedimentary and metasedimentary lithic fragments (13%–36%), with the average quartz–feldspar–lithic fragment (Q–F–L) ratio of 53:21:26. The point-count data of the analysed samples are shown in Table S2 (see the Supporting Information). Framework grain composition (Q–F–L) ternary plots indicate that the Lulehe Formation sandstones were mainly derived from a recycled orogenic source (Figure S1 in the Supporting Information). Besides, the framework grain compositions show variations in samples from different locations or in samples from different layers of the same section (Figures 8, 10a and S1; Table S2).

4.4 | Heavy minerals

Transparent heavy minerals in the analysed Lulehe Formation samples mainly consist of garnet, epidote, chlorite, tourmaline and zircon (Figures 7d and 9f). Similar to the framework grains, most heavy mineral grains are angular to subangular in shape. The ZTR index (proportions of zircon, tourmaline and rutile in all transparent heavy minerals, proposed by Hubert [1962]) and Stability index (the ratio of stable/unstable heavy minerals, proposed by Jian, Guan, Zhang, Zhang, et al. [2013]) are employed to indicate the degrees of sediment maturity. Most of these index values are moderate to low and are quite variable among the analysed samples (the ZTR index values range from 7 to 65, averaging 24 and the Stability index values range from 0.5 to 38, averaging 7, Figure 10b). Some samples (e.g., LS1-01 and LS1-02) are rich in zircon and tourmaline, whereas some other samples (e.g., LLH-30 and 16DHG-06) have comparatively low zircon and tourmaline contents and thus show high GZi (garnet–zircon index, $\text{GZi} = 100 \times \text{garnet} / (\text{garnet} + \text{zircon})$, proposed by Morton and Hallsworth [1994]) values (Table S3). All the

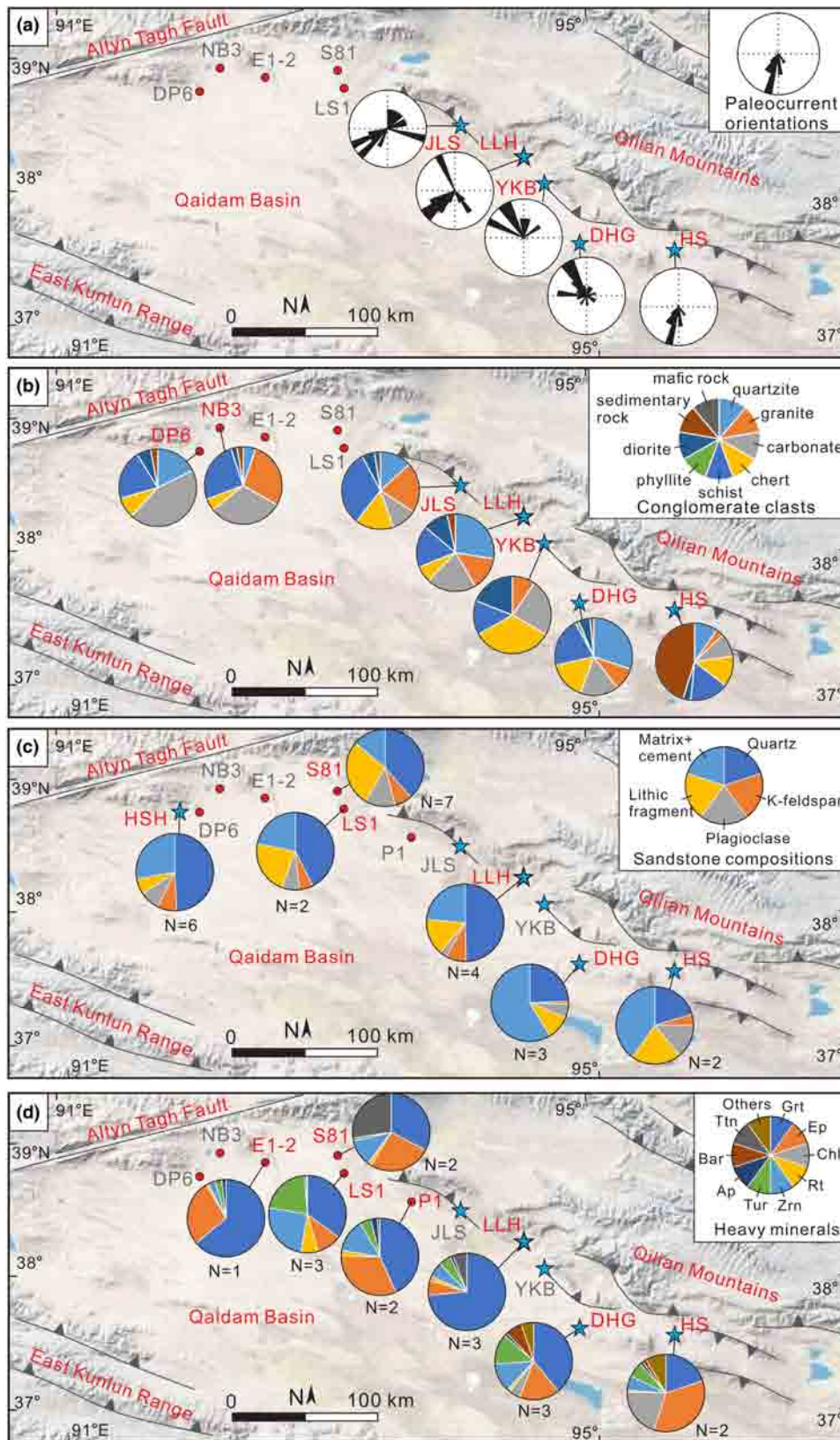


FIGURE 7 Paleocurrent orientation (a), conglomerate clast counting (b), petrographic (c) and heavy mineral assemblage (d) data of the Lulehe Formation strata in this study. Petrographic and heavy mineral average compositions of each section (or drilling well) are indicated and the capital N shows quantity of the analysed samples. Zrn: Zircon, tur: Tourmaline, ap: Apatite, Ttn: Titanite, Grt: Garnet, ep: Epidote, Chl: Chlorite, rt: Rutile, Bar: Baryte. The “others” involves hornblende, augite, biotite, staurolite. The petrographic data of samples from the HSH section are from Rieser et al. (2005). Red dot and blue pentagram symbols display locations of drilling wells and outcrop sections, respectively.

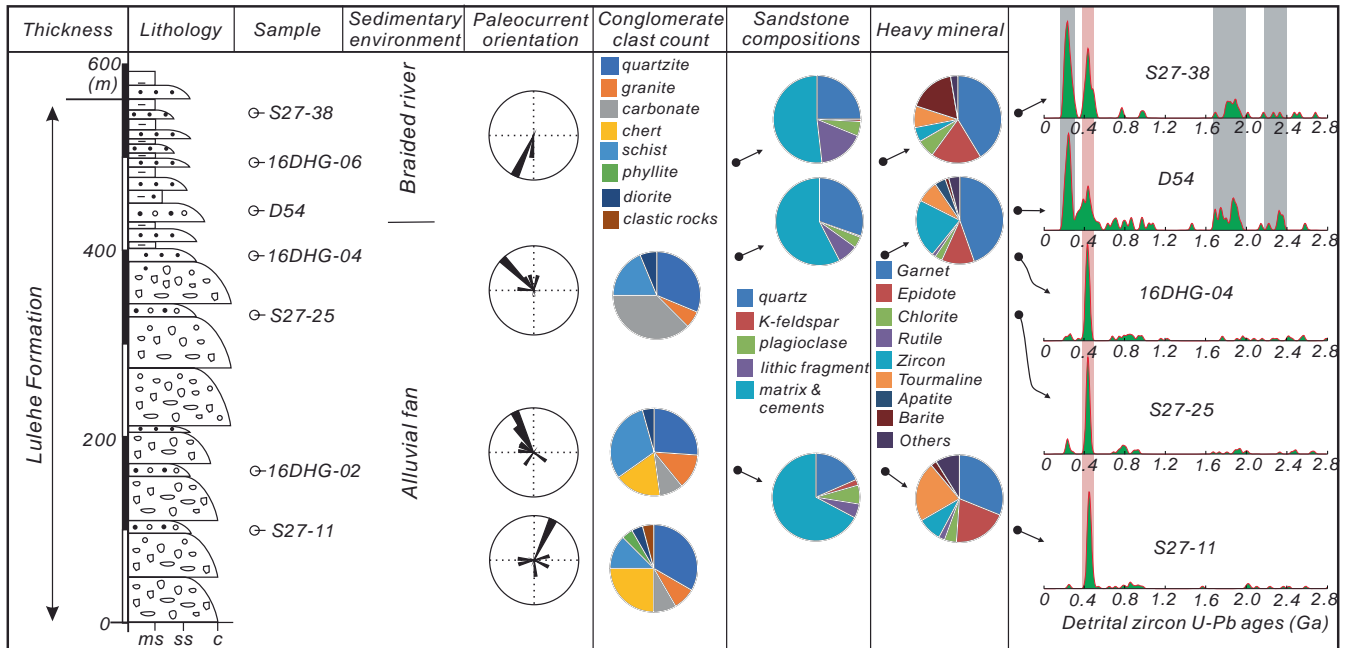


FIGURE 8 Stratigraphic variations of paleocurrent orientation, conglomerate clast composition, sandstone composition, heavy mineral and detrital zircon U-pb age data of the Lulehe Formation strata at the Dahonggou (DHG) section in the northern Qaidam basin. Detrital zircon age data of the samples D54, S27-11, S27-25 and S27-38 are from Wang et al. (2017) and Song et al. (2019). Note that the upper Lulehe Formation indicates different paleocurrent orientations, sandstone compositions and detrital zircon age populations from the lower Lulehe Formation. Ms: Mudstone, ss: Sandstone, c: Conglomerate.

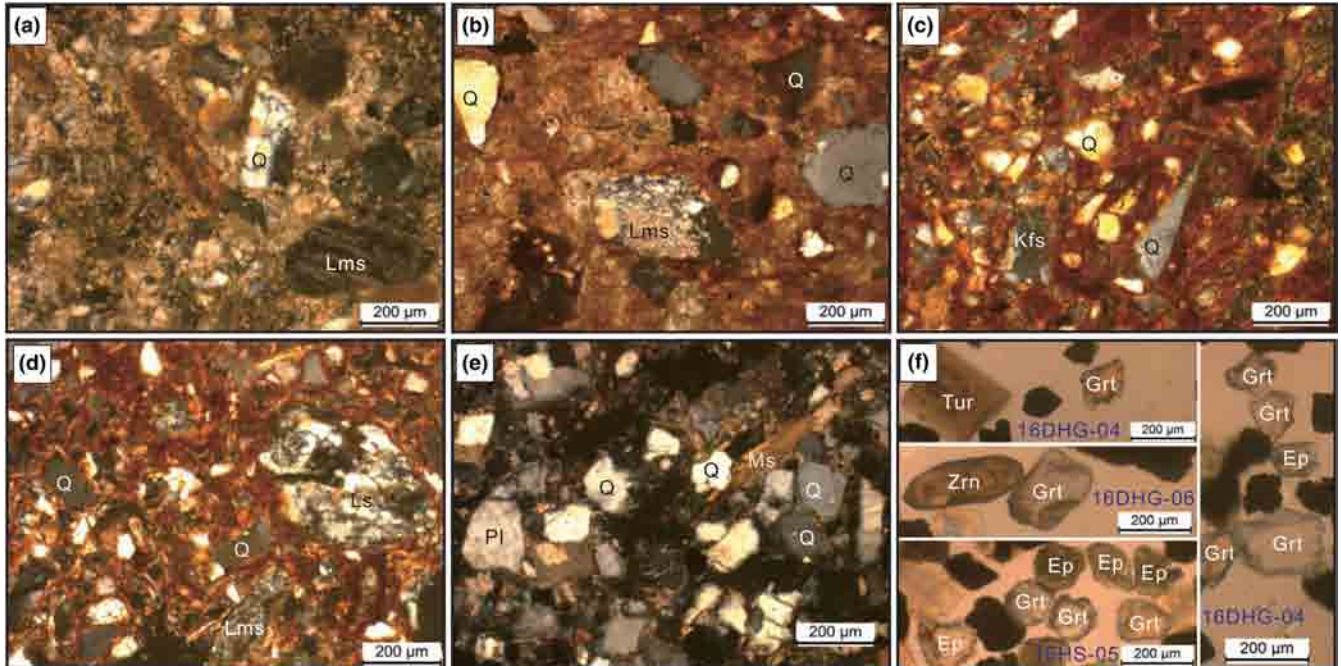


FIGURE 9 Representative photomicrographs for the Lulehe Formation sandstone samples (taken with cross-polarized light under a polarizing microscope) and representative heavy minerals (plane-polarized light) in these analysed samples. (a) 16HS-05; (b) 16DHG-02; (c) 16DHG-04; (d) LLH-28; (e) LLH-30; (f) heavy mineral grains. Note that most sandstones are matrix-supported, poorly sorted greywackes (e.g., A–D). The heavy mineral assemblages are dominated by garnet (Gr), epidote (ep), tourmaline (tur) and zircon (Zrn). Q: Quartz; Kfs: K-feldspar; pl: Plagioclase; ls: Sedimentary lithic fragments; Lms: Metasedimentary lithic fragments; Ms: Muscovite.

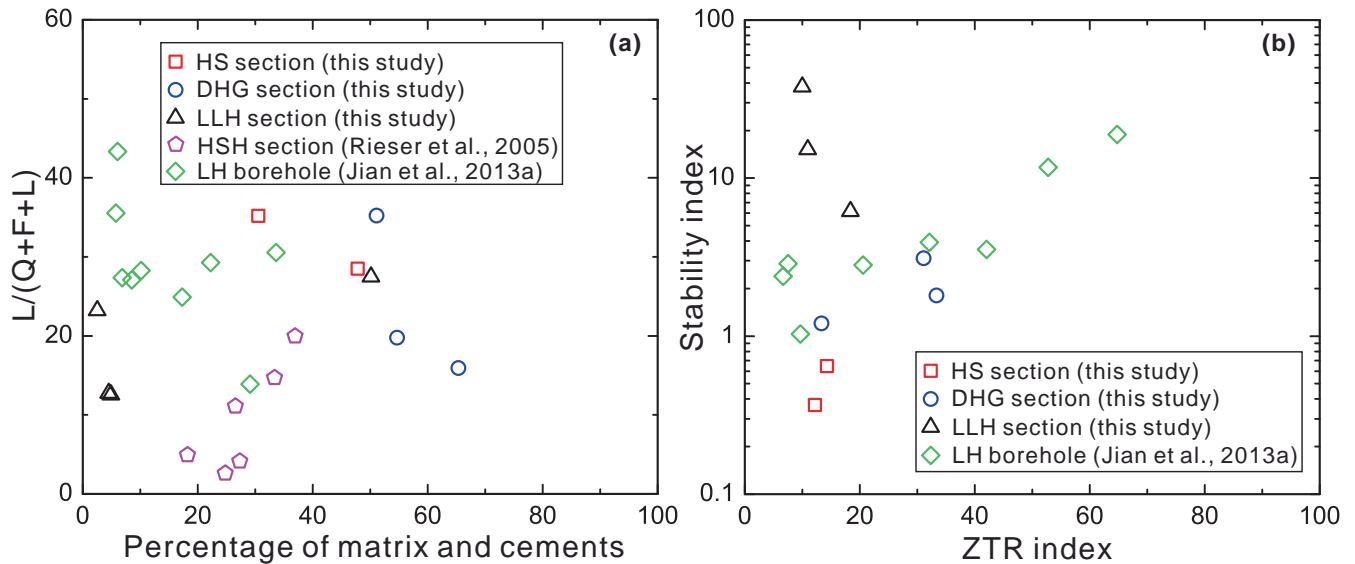


FIGURE 10 (a) Binary plots of matrix and cement percentages in bulk samples and lithic fragment percentages in the framework grain compositions (i.e., $L/(Q+F+L)$). Note that the Lulehe Formation sandstones from the northern Qaidam basin have variable abundances of matrix and cements and relatively high lithic fragment compositions, whereas the HSH section samples were reported to have low lithic fragment contents. (b) Heavy mineral maturity index values. ZTR index = $100 \times (\text{zircon} + \text{tourmaline} + \text{rutile}) / \text{all transparent heavy minerals}$; stability index = $(\text{zircon} + \text{tourmaline} + \text{rutile} + \text{garnet} + \text{titanite}) / (\text{apatite} + \text{epidote} + \text{chlorite} + \text{baryte} + \text{others})$. The HSH section and the LH core (borehole in the Lenghu fold belt) samples were previously analysed by Rieser et al. (2005) and Jian, Guan, Zhang, Zhang, et al. (2013), respectively. For the section and borehole locations, see Figure 1.

raw data and calculated index values of the transparent heavy minerals are shown in Table S3.

4.5 | Detrital zircon U–Pb ages

We report a total of 404 detrital zircon U–Pb ages from the 4 analysed Lulehe Formation sandstone samples, of which 371 U–Pb ages therein are concordant ages (see Figure S2 for the U–Pb Concordia diagram of each sample). The analysed detrital zircon crystals range from 50 to 250 μm (Table S4) and are dominantly subangular to angular in shape (Figure S3). Most (>90%) zircons in the samples are characterized by legible oscillatory zoning textures and have high Th/U ratios (>0.1) (Figure S3; Table S4). Only a few analysed zircon crystals with early Palaeozoic (400–500 Ma) and Neoproterozoic (750–850 Ma) ages have Th/U ratios <0.1 (Table S4).

Overall, detrital zircon U–Pb ages of the Lulehe Formation sandstone samples in this study primarily consist of 210–280 Ma; 390–480 Ma and 750–1000 Ma with subordinate Paleoproterozoic and Neoproterozoic ages. However, the 4 analysed samples display distinct detrital zircon age populations. The analysed detrital zircons of sample E1-2-01 are dominated by Phanerozoic ages (83%), with ranges of 220–280 Ma and 400–470 Ma, while the detrital zircons of sample 16DHG-04 mainly show early Palaeozoic ages (420–470 Ma, accounting for 51 in 94 concordant ages) (Figure 11). The detrital zircon ages of sample 16HS-05 are comparatively

various (Figure 11), including 210–260 Ma, 420–480 Ma, 1800–2000 Ma and 2300–2800 Ma. Detrital zircon grains in this sample (16HS-05) also have a certain percentage of early Permian–Late Devonian (280–380 Ma, accounting for 10 in 90) ages (Figure 11). While Neoproterozoic ages are minor in detrital zircons of these 3 samples, zircons in sample LLH-30 are featured by middle Neoproterozoic (730–830 Ma) ages (Figure 11). Zircons with Phanerozoic ages (240–260 Ma and 400–450 Ma) only account for 33% of the analysed crystals in sample LLH-30 (Figure 11). The details about the U–Th–Pb isotopic ratios and ages of all the analysed zircon crystals are shown in Table S4. All the new data and previously reported detrital zircon age data of the Lulehe Formation strata from the Qaidam basin are illustrated as Kernel density estimation (KDE) plots in Figure S4 (Supporting Information) and the corresponding cumulative probability curves and non-metric multi-dimensional scaling (MDS) plots are shown in Figure 12 for comparison.

5 | DISCUSSION

5.1 | Provenance of the Lulehe Formation sedimentary rocks in the Qaidam basin

Our results demonstrate that the analysed Lulehe Formation sedimentary rocks from different locations

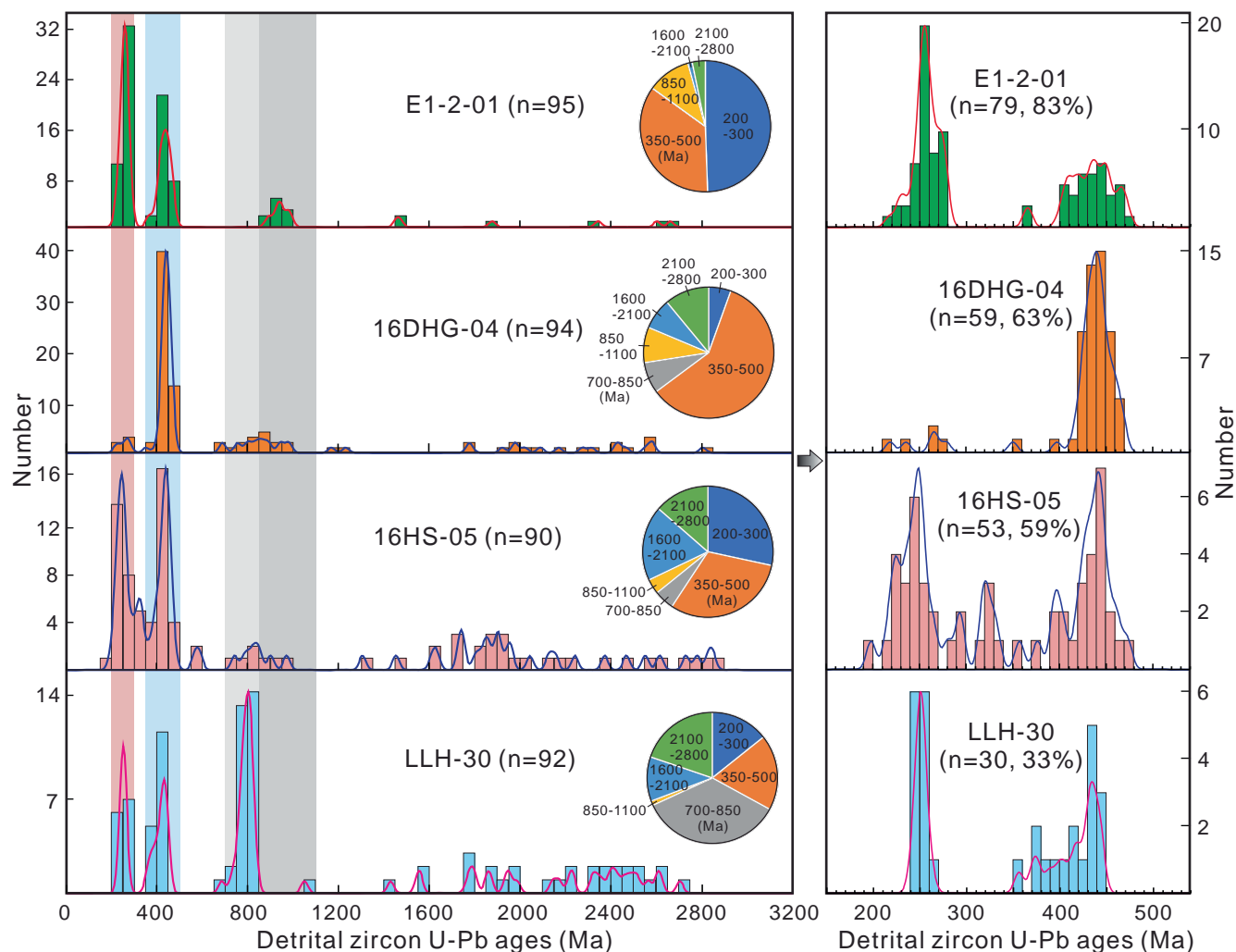


FIGURE 11 Detrital zircon U–pb age distributions of the analysed Lulehe Formation samples. All-age kernel density estimation (KDE) plots (left) were drawn by using bandwidth = 15 in the DensityPlotter program (Vermeesch, 2012), while the phanerozoic-age plots (right) were drawn by using bandwidth = 5.

have diverse detrital compositions (including conglomerate clasts, sandstone framework grains, heavy minerals (Figure 7) and detrital zircon U–Pb age populations (Figure 11)), implying distinct source regions and different parent-rock types. The spatially diverse sediment sources are also reinforced by the dissimilar paleocurrent orientations (Figure 7a). On the whole nevertheless, the dominance of schist, phyllite and quartzite clasts in the conglomerates, and high abundances of metamorphic lithic fragments in framework grains (Figures 7c and 9a–e) and garnet, epidote and chlorite in heavy minerals (Figures 7d and 9f; Table S3) of the sandstone samples indicate predominant contributions of metamorphic rocks. This is consistent with the dominant role of metamorphic rocks in the Qilian Mountains. Given that the Qaidam basin crystalline basement and the North Qaidam–South Qilian belts show well-marked 230–290 Ma zircon age signatures (Figure 6; Cheng et al., 2017; Zhang et al., 2021), the Permian–Triassic detrital zircon crystals in the

Lulehe Formation sandstone samples from the northern Qaidam basin could be derived from related zircon-rich rocks in these adjacent regions, rather than those widespread Permian–Triassic granitoid rocks in the Eastern Kunlun Range. Sandstones from the LLH section and the Suganhu regions indicate remarkable early–middle Neoproterozoic zircon age (with the peaks of ca. 850 Ma) populations (Figure 13), indicating prominent sediment supply from the Neoproterozoic basement rocks in west part of the Qilian Mountains. It is interesting that some detrital zircon grains with ages of 280–380 Ma are present in the sample 16HS-05 (Figure 11), which is quite different from other Lulehe Formation samples. As some Permian–Triassic siliciclastic sedimentary strata in the adjacent regions indicate remarkable late Palaeozoic zircon age signatures (Jian, Weislogel, et al., 2019; Li, Chen, et al., 2020), recycling of these sedimentary strata might contribute 280–380 Ma detrital zircon grains. The interpretation is supported by the occurrence of sandstone,

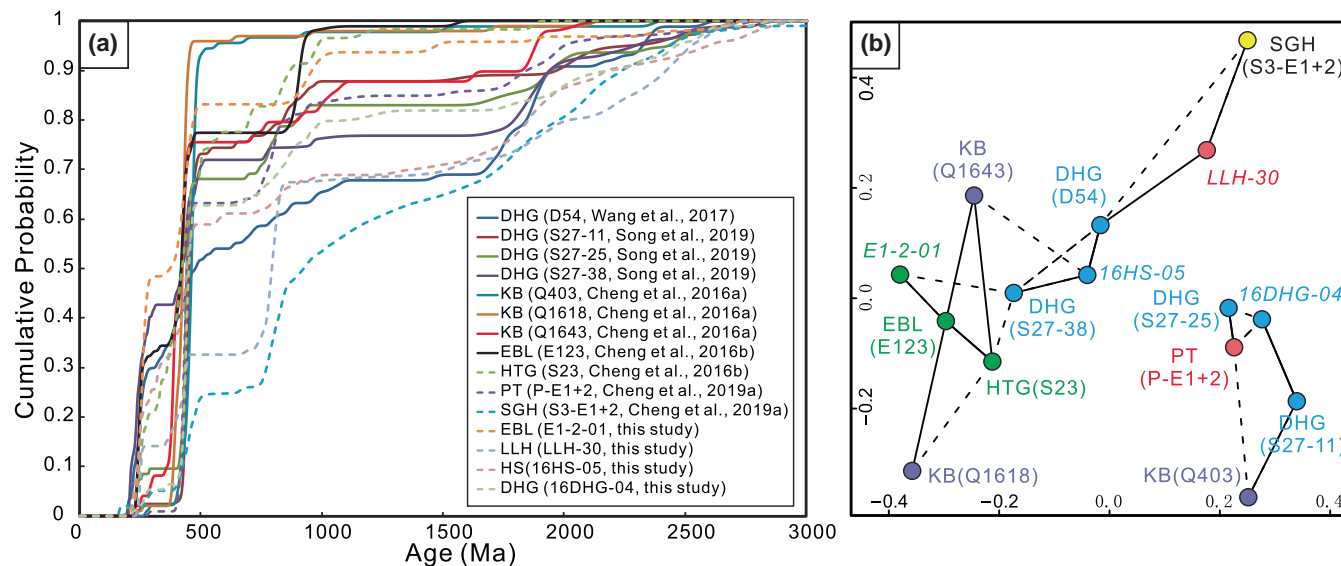


FIGURE 12 (a) Detrital zircon U–pb age cumulative probability plots and (b) non-metric multi-dimensional scaling (MDS) plots for the Lulehe Formation sandstones from the Qaidam basin. The MDS plots were drawn by the R programming language-based provenance software (Vermeesch et al., 2016). Solid lines and dashed lines in the MDS plots indicate the closest and second closest neighbours, respectively. Data are from both this study (Table S4) and previous studies (Table S5; Cheng, Fu, et al., 2016; Cheng, Garziona, Mitra, et al., 2019; Cheng, Jolivet, et al., 2016; Wang et al., 2017; Song et al., 2019). For all the detrital zircon dating sample locations, see Figure 6a.

mudstone and carbonate rock clasts in the conglomerates (Figure 7b) and sedimentary lithic fragments in the angular to subangular, poorly sorted sandstones (Figure 9), which reflect localized sources, short transport distances, high-gradient depositional processes and potential recycling of pre-Cenozoic sedimentary successions (e.g., Carboniferous–Triassic oceanic sedimentary sequences and Jurassic and Cretaceous siliciclastic rocks). This is also consistent with a recent argument that noncrystalline basement rocks in the nearby fold-and-thrust belts cannot be overlooked when seeking potential source areas for the Cenozoic Qaidam basin (Lu et al., 2018). Collectively, we favour that the Lulehe Formation coarse-grained deposits in the northern Qaidam basin were supplied by relatively high-relief regions that were close to the depositional areas, such as related regions in the North Qaidam–South Qilian metamorphic belts and the interior of the Qaidam basin (containing pre-Cenozoic crystalline and noncrystalline basement rocks), rather than the southern distant Qimantagh and Eastern Kunlun regions, not as previously recommended in some literatures (Bush et al., 2016; Nie et al., 2020; Wang et al., 2017).

Furthermore, several Lulehe Formation sandstone samples from the HSH section (northwestern Qaidam basin, Figure 1b) were reported to have high quartz and feldspar contents and very low lithic fragment contents (Rieser et al., 2005; Figures 7c and 10a). A great number of borehole Lulehe Formation samples from southwestern Qaidam basin indicate relatively high zircon, leucosene, hornblende, epidote and garnet contents in heavy

mineral assemblages (Zhu et al., 2017). Previous published detrital garnet geochemical data of the sample S81-01 (northwestern Qaidam basin, Figure 1c) demonstrate that these garnet grains were sourced from intermediate-acidic igneous rocks and low-, medium-grade metapelites (Hong et al., 2020; Jian, Guan, Zhang, Zhang, et al., 2013). All these reported results suggest contributions of both igneous and metamorphic rocks to the Lulehe Formation sediments in west part of the Qaidam basin. This is consistent with the lithological settings of the Eastern Kunlun and southern Altun Ranges. Detrital zircon age data of the Lulehe Formation strata from the EBL, HTG and KB regions (Cheng, Fu, et al., 2016; Cheng, Jolivet, et al., 2016; Figures 6 and 13) also support the major detritus contributions from local regions in these ranges or within the Qaidam terrane. Specifically, detrital zircon grains of the EBL and HTG samples are featured by 230–280 Ma, 400–480 Ma and 850–1000 Ma age clusters (Figure 13a) and were most likely derived from the adjacent Neoproterozoic early Palaeozoic and Permian–Triassic granitoids within the Qaidam terrane or in the Altun Range (Figure 6), whereas the dominance of 380–480 Ma zircon grains in the KB samples (Figure 13a) indicate possible contributions of the local Ordovician–Devonian granitoids in the Qimantagh regions (west part of the Eastern Kunlun Range, Figure 6). In a word, all the detrital composition data in this study and previous studies suggest diverse sediment sources and small sediment-routing systems for those Cenozoic basal deposits in the Qaidam basin. The provenance interpretation is

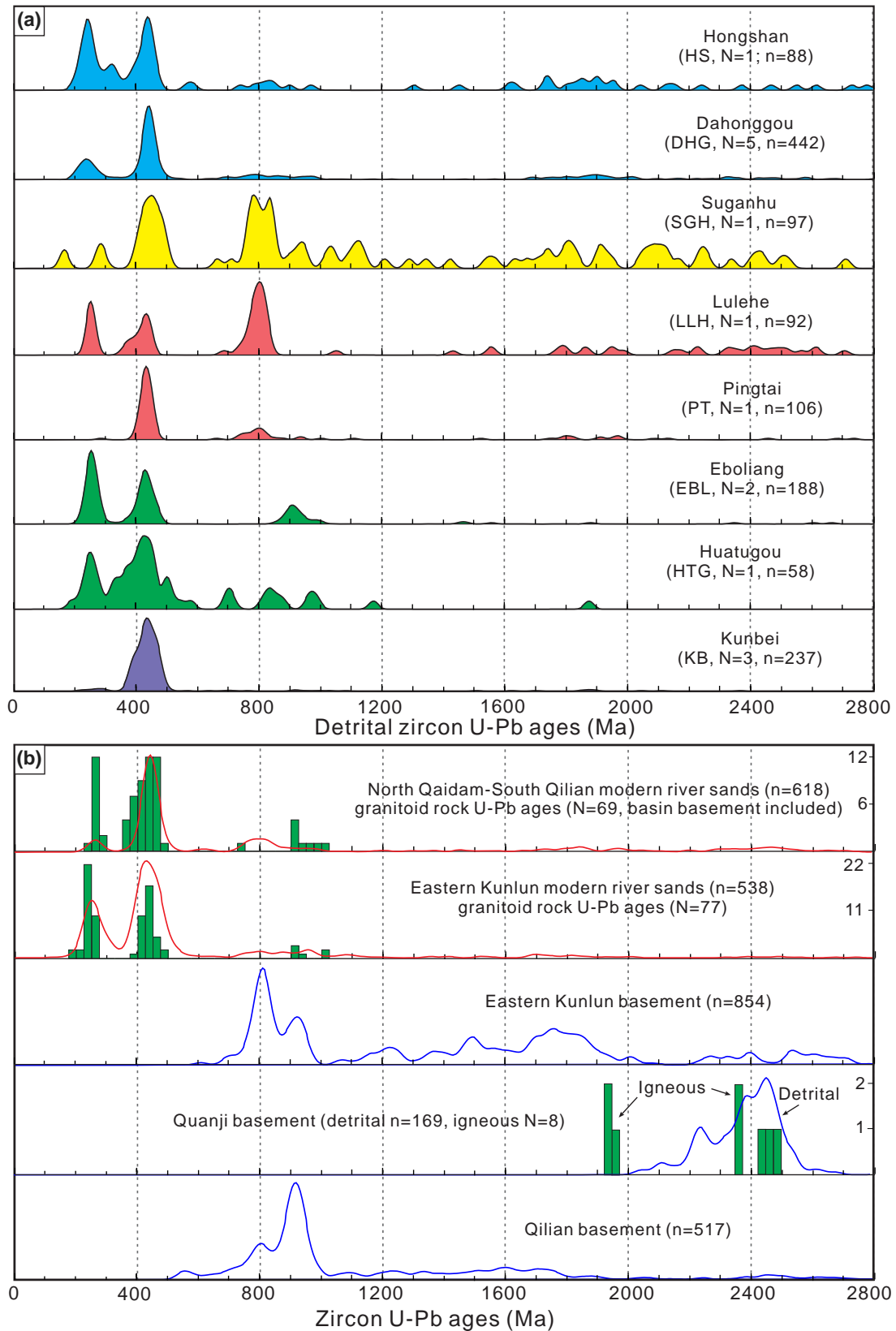


FIGURE 13 Detrital zircon U-pb age KDE plots (bandwidth = 15) of (a) the Lulehe Formation sandstones and (b) the potential source regions (red curves: Modern river sands; blue curves: Precambrian sedimentary rocks; the histograms: Published zircon U-pb ages of granitoids). The modern river sand data are from Lease et al. (2007), Liu et al. (2012), Li et al. (2013), McRivette et al. (2019), Song et al. (2019), Wu, Zuzi, et al. (2019) and Zhang et al. (2021). The Precambrian basement data are from Gehrels et al. (2003a, 2011), Xu et al. (2007), Wang, Chen, et al. (2008), Chen et al. (2009, 2012), Yu, Guo, et al. (2017), Yu et al. (2019) and Jian, Weislogel, et al. (2019, 2020).

consistent with the results from flexural modelling which show that topographic load generated by both the Qilian Mountains and the Eastern Kunlun Range may be responsible for the subsidence of the Qaidam basin regions during the deposition of the Lulehe Formation (Cheng, Garzione, Jolivet, et al., 2019).

Our results also reveal vertical compositional changes among the Lulehe Formation sedimentary rocks from a single outcrop section (Figure 8), implying temporal variations in sediment provenance of the Lulehe Formation strata. Take the DHG section as an example, samples from the sandstone interlayers within lower massive conglomerate beds have dominant early Palaeozoic (420–500 Ma) detrital zircon ages, whereas the upper sandstone samples exhibit more diverse detrital zircon age populations, including Permian–Triassic, early Palaeozoic, Neoproterozoic and abundant Paleoproterozoic (1670–2000 Ma and 2300–2500 Ma) ages (Figure 8). Given the characteristic Paleoproterozoic age signatures of the Quanji massif (Figures 6a and 13b), as mentioned above, and the varied paleocurrent orientations (from north- and northwest-directed to south-directed, Figure 8), we favour a sediment source change from a local and proximal region to the south (within the interior of the Qaidam basin) to a relatively broad and distant region in the North Qaidam–South Qilian belts during the depositional period. The interpretation is supported by the petrographic and heavy mineral data which show that the upper sandstone samples have comparatively abundant metamorphic lithic fragments and heavy minerals of metamorphic origin (e.g., garnet, epidote and chlorite) (Figure 8). In addition, those sandstones show relatively higher compositional maturity (e.g., lower abundance of matrix components) than the sandstones from the lower layers (Figure 8).

5.2 | Distribution and depositional process of the Lulehe Formation conglomerate-dominated, coarse-grained red beds in the Qaidam basin

While the Lulehe Formation outcrops are mainly present in the northern margin of the basin (Figure 1c), available drilling well and seismic data demonstrate that the Lulehe Formation strata are widespread within the basin and have highly varied thicknesses (0–1500 m) in different locations (Figures 4 and 5). Specifically, the Lulehe Formation strata are generally absent in east part and south margin of the current Qaidam basin, which are quite different from the spatial distributions of other Cenozoic stratigraphic units (Bao et al., 2017). And the thickest Lulehe Formation strata (>1000 m) are present in Lenghu and Eboliang regions

(Figure 1c) in the northern Qaidam basin (Figure 4; Bao et al., 2017; Cheng, Garzione, Jolivet, et al., 2019). Note that several drilling wells (e.g., Well MB3, Figure 4) from the Maxian belt (the Maxian regions (Figure 1c) are interpreted as an Eocene paleohigh [Jian, Zhang, et al., 2019]) in the northern Qaidam basin indicate that the Xia Ganchaigou Formation strata directly overlie pre-Cenozoic crystalline basement (Figures 4 and 5). In addition to the Maxian paleohigh, several paleohighs, which are bounded by reverse faults and have thin Lulehe Formation strata (<100 m), have been identified in the Qaidam basin (e.g., Cao et al., 2018; Zeng et al., 2018). The noteworthy diversity in sediment thickness (Figure 4) and the occurrence of paleohighs, growth strata and stratigraphic onlap phenomena (Figure 5) imply that the Qaidam regions were most likely under highland-erosion and lowland-deposition conditions when the Cenozoic sedimentation initiated. All the evidence points to the conclusion that these coarse-grained red beds accumulated separately and the Qaidam terrane was most likely present as several isolated depocenters, rather than a coherent basin, at the beginning of the Cenozoic deposition (Figure 14). This conclusion is reinforced by the above provenance interpretation, that is various, localized, proximal sediment sources for the Lulehe Formation. Those paleohighs within the Qaidam basin could be erosion regions to provide detritus for adjacent depocenters (Figure 14). The presence of isolated depositional areas also implies that the Cenozoic basal coarse-grained red beds in different regions might have different depositional ages. In this case, the dissimilar depositional ages for the Lulehe Formation strata from different regions (e.g., Fang, Galy, et al., 2019; Ji et al., 2017; Nie et al., 2020; Wang et al., 2017) all seem reasonable and may reveal that the Lulehe Formation depositional processes were diachronous across the basin. Previously reported paleomagnetic data of these red beds indicate relatively high sedimentation rates (>ca. 100 m/Ma) (Fang, Galy, et al., 2019; Ji et al., 2017), revealing rapid sediment supply and/or enhanced basin subsidence. The Lulehe Formation from the northern Qaidam basin is interpreted as a synorogenic conglomerate-dominated bed deposited by high-gradient depositional systems (such as proximal alluvial and fluvial environments) (Cheng, Garzione, Jolivet, et al., 2019; Guan & Jian, 2013; Zhuang et al., 2011), while the Lulehe Formation within the interior of the basin and in the southern margin of the basin is considered to be likely deposited in distal fluvial to marginal lacustrine environments (Cheng, Garzione, Jolivet, et al., 2019). All the distribution characteristics and depositional process explanations are consistent with the compositional results of

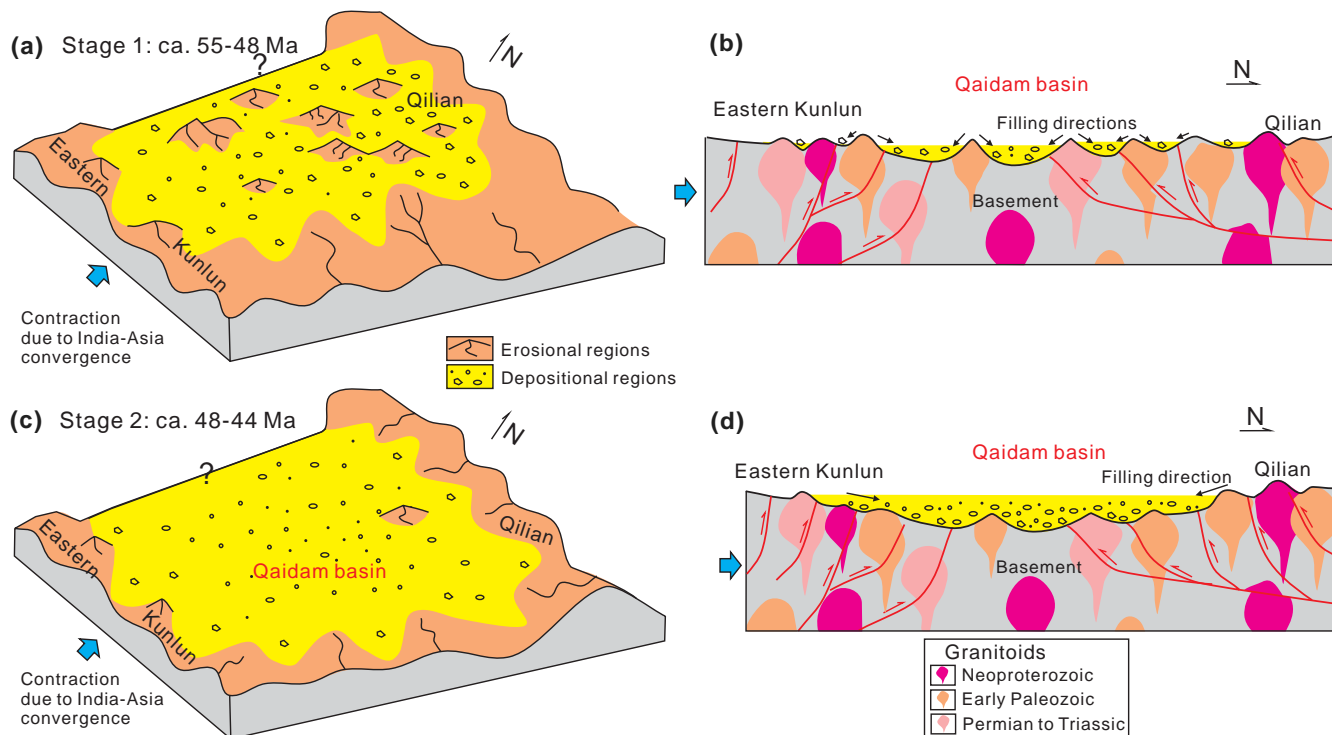


FIGURE 14 Two-stage sedimentary filling model for deposition of the Lulehe Formation in the Qaidam basin. (a) and (b) stage 1 (ca. 55–48 Ma): Initiation of the Cenozoic deposition in the Qaidam basin, shortly after the India-Eurasia collision. The Qaidam terrane was rendered as several isolated depocenters, dominated by matrix-supported conglomerates with nearby sources. In addition to the present-day Qilian and eastern Kunlun ranges, several high-relief regions of pre-Cenozoic basin basements also served as erosional terranes feeding coarse-grained sediments to the depositional areas. This resulted in variable paleocurrent directions and highly diverse detrital compositions for the lower Lulehe Formation sedimentary succession. (c) and (d) stage 2 (ca. 48–44 Ma): A single middle Eocene basin, serving as the precursor of the Cenozoic Qaidam basin, with sediments (including conglomerates, sandstones and minor siltstones and mudstones) derived from the surrounding relatively high-relief regions to the north, east and south.

conglomerate and sandstone samples and corresponding provenance interpretations.

5.3 | Eocene contractional deformation and sedimentary basin development in northern Tibet as a far-field, fast response to the India-Eurasia collision

Although many structures around the Qaidam basin were dated to initiate in the middle–late Miocene (e.g., George et al., 2001; Zheng et al., 2010; Zhuang et al., 2018), a growing number of thermochronological and structural analysis evidence suggests that extensive deformation occurred across the northern Tibet during the Eocene (An et al., 2020; Clark et al., 2010; Li, Zuza, et al., 2020; Yin, Dang, Wang, et al., 2008; Yuan et al., 2013; Zhang et al., 2020), that is, shortly after the India-Eurasia collision. Detrital thermochronological data demonstrate a rapid and short-lived early Eocene cooling event in the source regions of the Cenozoic Qaidam basin (He

et al., 2021; Jian et al., 2018; Wang et al., 2015). Previous geological mapping results and seismic profile interpretations demonstrate that the southernmost part of the Qilian Mountains and contractional structures (e.g., the South Qilian and North Qaidam thrust belts) along the northern margin of Qaidam basin initiated in the Palaeocene-early Eocene (Yin, Dang, Wang, et al., 2008). And early shortening in the Qilian Mountains may generate more reasonable crustal thickening rates (Zuza et al., 2019) than Miocene-initiated shortening as those research groups proposed. The high-quality 3D seismic data indicate that several reverse faults (e.g., the Niubei and Maxian Faults, Figure 5) within the basin were active during the depositional period of the Lulehe Formation. Our provenance analysis results and depositional process interpretations advocate that the Lulehe Formation had localized, proximal detritus sources and the deposition was constricted to relatively small drainage catchments (Figure 14). All the evidence suggests that the early Cenozoic Qaidam basin developed in a contractional tectonic setting and the early Eocene contractional deformation regime and initiation of the Cenozoic deposition in the Qaidam basin were

most likely a far-field, fast response to the India-Eurasia collision.

In addition to the Qaidam basin, several nonmarine basins (e.g., Xining, Linxia, Nangqian, Gonjo and Mula basins) in the northern and eastern Tibetan Plateau are also characterized by coarse-grained, poorly sorted red beds for the Cenozoic basal sedimentary strata (Dai et al., 2006; Horton et al., 2002; Jackson Jr et al., 2018; Tang et al., 2017 and references therein; Feng et al., 2022 and references therein). These Cenozoic basal red beds have similar textures and depositional ages to the Lulehe Formation in the Qaidam basin. Those Eocene-initiated basins are dominantly bounded by syn-sedimentary thrusts (Figure S5; Horton et al., 2002, 2004; Jackson Jr et al., 2020; Jin et al., 2018; Spurlin et al., 2005; Studnicki-Gizbert et al., 2008; Yin & Harrison, 2000). Most of these thrust systems are concentrated along pre-Cenozoic suture zones (e.g., the early Palaeozoic Qilian suture and the Late Triassic Ganzi-Litang suture) (Jackson Jr et al., 2020; Zuza et al., 2018, 2019). Field-based observations from a geological traverse across the Qilian Mountains demonstrate that the Cenozoic evolution of northern Tibet is similar to that of the Himalaya; both involving large-scale underthrusting of mantle lithosphere beneath Tibet (Zuza et al., 2019). The early Cenozoic reactivation of these old suture zones was most likely driven by plate boundary interactions between India and Eurasia (Jackson Jr et al., 2020; Zuza et al., 2018, 2019). Although pre-collisional deformation and crustal thickening in the plateau have been adequately recognized (Jian et al., 2018; Kapp et al., 2005, 2007; Rohrmann et al., 2012; Volkmer et al., 2007; Wang, Zhao, et al., 2008), it has been well accepted that Cenozoic deformation throughout most of the plateau was underway not long after the collision (Yuan et al., 2013 and references therein). The sedimentary response in the Qaidam basin and other Cenozoic nonmarine basins (Figure S5) implies that the northern and eastern boundary of the plateau was established once the India-Eurasia collision commenced and contractional deformation caused by collision propagated to the regions far away from the collisional zone shortly after the collision, supporting the synchronous deformation models for the growth of the plateau.

6 | CONCLUSIONS

An integrated provenance analysis for the Cenozoic Lulehe Formation coarse-grained red beds in the Qaidam basin, northern Tibet, allows for a better understanding of sedimentation-tectonics feedback processes and how Cenozoic deposition started in the region. Results demonstrate that the Lulehe Formation in different locations

display dissimilar paleocurrent orientations, are compositionally and texturally immature and have distinct detrital compositions. We propose that Cenozoic deposition in the Qaidam basin initiated under contractional tectonic settings and the red beds were derived from localized, spatially diverse source rocks with relatively small drainage networks. We use the Qaidam basin and other Cenozoic nonmarine basins in the northern and eastern Tibet to suggest the development of these basins as a far-field, fast response to the India-Eurasia collision. Our findings favour that the synchronous contractional deformation throughout most of the plateau was underway shortly after the India-Eurasia collision.

ACKNOWLEDGEMENTS

This research was supported by the National Natural Science Foundation of China (Nos. 41902126, 41806052) and Xiamen University Fundamental Research Funds for the Central Universities (Nos. 20720190097, 20720190103). We appreciate the consistent support from the PetroChina Qinghai Oilfield Company. We would like to thank Hanghai Liang, Dongming Hong and Shuo Zhang of Xiamen University for their help in sample collection and lab analysis. This work benefited from constructive comments by Andrew Zuza, Xiangjiang Yu, Will Jackson and two anonymous reviewers. Xing Jian designed the study. Xing Jian, Ling Fu and Ping Guan collected the outcrop and borehole samples. Xing Jian, Ping Wang, Wei Zhang, Hanjing Fu and Haowei Mei analysed samples and obtained the data. Xing Jian wrote the draft and all authors edited the paper.

CONFLICT OF INTEREST

No conflict of interest is declared.

DATA AVAILABILITY STATEMENT

All the supporting data are available in the Supporting Information files.

REFERENCES

- An, K., Lin, X., Wu, L., Yang, R., Chen, H., Cheng, X., Xia, Q., Zhang, F., Ding, W., Gao, S., Li, C., & Zhang, Y. (2020). An immediate response to the Indian-Eurasian collision along the northeastern Tibetan plateau: Evidence from apatite fission track analysis in the Kuantan Shan-Hei Shan. *Tectonophysics*, 774, 228278. <https://doi.org/10.1016/j.tecto.2019.228278>
- Andersen, T. (2002). Correction of common lead in U-pb analyses that do not report ²⁰⁴Pb. *Chemical Geology*, 192, 59–79. [https://doi.org/10.1016/S0009-2541\(02\)00195-X](https://doi.org/10.1016/S0009-2541(02)00195-X)
- Bao, J., Wang, Y., Song, C., Feng, Y., Hu, C., Zhong, S., & Yang, J. (2017). Cenozoic sediment flux in the Qaidam Basin, northern Tibetan plateau, and implications with regional tectonics and climate. *Global and Planetary Change*, 155, 56–69. <https://doi.org/10.1016/j.gloplacha.2017.03.006>

- Bush, M. A., Saylor, J. E., Horton, B. K., & Nie, J. (2016). Growth of the Qaidam Basin during Cenozoic exhumation in the northern Tibetan plateau: Inferences from depositional patterns and multiproxy detrital provenance signatures. *Lithosphere*, 8(1), 58–82. <https://doi.org/10.1130/L449.1>
- Cao, Z., Sun, X., Wu, W., Tian, G., Zhang, S., Li, H., Sun, Z., Xu, L., & Wang, R. (2018). Formation and evolution of thrust paleo-uplift at the margin of Qaidam basin and its influences on hydrocarbon accumulation. *Acta Petrolei Sinica*, 39(9), 980–989 (In Chinese with English abstract). <https://doi.org/10.7623/syxb201809003>
- Chen, F. H., Chen, J. H., Holmes, J., Boomer, I., Austin, P., Gates, J. B., Wang, N. L., Brooks, S. J., & Zhang, J. W. (2010). Moisture changes over the last millennium in arid Central Asia: A review, synthesis and comparison with monsoon region. *Quaternary Science Reviews*, 29, 1055–1068. <https://doi.org/10.1016/j.quascirev.2010.01.005>
- Chen, N., Gong, S., Sun, M., Li, X., Xia, X., Wang, Q., Wu, F., & Xu, P. (2009). Precambrian evolution of the Quanji block, northeastern margin of Tibet: Insights from zircon U–pb and Lu–hf isotope compositions. *Journal of Asian Earth Sciences*, 35, 367–376. <https://doi.org/10.1016/j.jseae.2008.10.004>
- Chen, N., Zhang, L., Sun, M., Wang, Q., & Kusky, T. M. (2012). U–pb and hf isotopic compositions of detrital zircons from the paragneisses of the Quanji massif, NW China: Implications for its early tectonic evolutionary history. *Journal of Asian Earth Sciences*, 54, 110–130. <https://doi.org/10.1016/j.jseae.2012.04.006>
- Chen, N. S., Liao, F. X., Wang, L., Santosh, M., Sun, M., & Wang, Q. Y. (2013). Late Paleoproterozoic multiple metamorphic events in the Quanji massif: Links with Tarim and North China cratons and implications for assembly of the Columbia supercontinent. *Precambrian Research*, 228, 102–116. <https://doi.org/10.1016/j.precamres.2013.01.013>
- Cheng, F., Fu, S., Jolivet, M., Zhang, C., & Guo, Z. (2016). Source to sink relation between the eastern Kunlun range and the Qaidam Basin, northern Tibetan plateau, during the Cenozoic. *GSA Bulletin*, 128(1–2), 258–283. <https://doi.org/10.1130/B31260.1>
- Cheng, F., Garzzone, C. N., Jolivet, M., Guo, Z., Zhang, D., Zhang, C., & Zhang, Q. (2019). Initial deformation of the northern Tibetan plateau: Insights from deposition of the Lulehe formation in the Qaidam Basin. *Tectonics*, 38(2), 741–766. <https://doi.org/10.1029/2018TC005214>
- Cheng, F., Garzzone, C. N., Mitra, G., Jolivet, M., Guo, Z., Lu, H., Li, X., Zhang, B., Zhang, C., Zhang, H., & Wang, L. (2019). The interplay between climate and tectonics during the upward and outward growth of the Qilian Shan orogenic wedge, northern Tibetan plateau. *Earth-Science Reviews*, 198, 102945. <https://doi.org/10.1016/j.earscirev.2019.102945>
- Cheng, F., Jolivet, M., Fu, S., Zhang, C., Zhang, Q., & Guo, Z. (2016). Large-scale displacement along the Altyn Tagh Fault (North Tibet) since its Eocene initiation: Insight from detrital zircon U–Pb geochronology and subsurface data. *Tectonophysics*, 677–678, 261–279. <https://doi.org/10.1016/j.tecto.2016.04.023>
- Cheng, F., Jolivet, M., Guo, Z., Wang, L., Zhang, C., & Li, X. (2021). Cenozoic evolution of the Qaidam basin and implications for the growth of the northern Tibetan plateau: A review. *Earth-Science Reviews*, 220, 103730. <https://doi.org/10.1016/j.earscirev.2021.103730>
- Cheng, F., Jolivet, M., Hallot, E., Zhang, D., Zhang, C., & Guo, Z. (2017). Tectono-magmatic rejuvenation of the Qaidam craton, northern Tibet. *Gondwana Research*, 49, 248–263. <https://doi.org/10.1016/j.gr.2017.06.004>
- Clark, M. K. (2012). Continental collision slowing due to viscous mantle lithosphere rather than topography. *Nature*, 483(7387), 74–77. <https://doi.org/10.1038/nature10848>
- Clark, M. K., Farley, K. A., Zheng, D., Wang, Z., & Duvall, A. R. (2010). Early Cenozoic faulting of the northern Tibetan plateau margin from apatite (U–Th)/He ages. *Earth and Planetary Science Letters*, 296(1–2), 78–88. <https://doi.org/10.1016/j.epsl.2010.04.051>
- Dai, S., Fang, X., Dupont-Nivet, G., Song, C., Gao, J., Krijgsman, W., Langereis, C., & Zhang, W. (2006). Magnetostratigraphy of Cenozoic sediments from the Xining Basin: Tectonic implications for the northeastern Tibetan plateau. *Journal of Geophysical Research: Solid Earth*, 111, B11102. <https://doi.org/10.1029/2005JB004187>
- Dayem, K. E., Molnar, P., Clark, M. K., & Houseman, G. A. (2009). Far-field lithospheric deformation in Tibet during continental collision. *Tectonics*, 28(6), TC6005. <https://doi.org/10.1029/2008TC002344>
- Dickinson, W. R. (1985). Interpreting provenance relations from detrital modes of sandstones. In *Provenance of arenites* (pp. 333–361). Springer.
- Du, D. D., Zhang, C. J., Mughal, M. S., Wang, X. Y., Blaise, D., Gao, J. P., Ma, Y., & Luo, X. R. (2018). Detrital apatite fission track constraints on Cenozoic tectonic evolution of the northeastern Qinghai-Tibet plateau, China: Evidence from Cenozoic strata in Lulehe section, northern Qaidam Basin. *Journal of Mountain Science*, 15(3), 532–547. <https://doi.org/10.1007/s11629-017-4692-5>
- Fang, X., Fang, Y., Zan, J., Zhang, W., Song, C., Appel, E., Meng, Q., Miao, Y., Dai, S., Lu, Y., & Zhang, T. (2019). Cenozoic magnetostratigraphy of the Xining Basin, NE Tibetan plateau, and its constraints on paleontological, sedimentological and tectonomorphological evolution. *Earth-Science Reviews*, 190, 460–485. <https://doi.org/10.1016/j.earscirev.2019.01.021>
- Fang, X., Galy, A., Yang, Y., Zhang, W., Ye, C., & Song, C. (2019). Paleogene global cooling-induced temperature feedback on chemical weathering, as recorded in the northern Tibetan plateau. *Geology*, 47(10), 992–996. <https://doi.org/10.1130/G46422.1>
- Feng, Z., Zhang, W., Fang, X., Zan, J., Zhang, T., Song, C., & Yan, M. (2022). Eocene deformation of the NE Tibetan plateau: Indications from magnetostratigraphic constraints on the oldest sedimentary sequence in the Linxia Basin. *Gondwana Research*, 101, 77–93. <https://doi.org/10.1016/j.gr.2021.07.027>
- Fu, H., Jian, X., Liang, H., Zhang, W., Shen, X., & Wang, L. (2022). Tectonic and climatic forcing of chemical weathering intensity in the northeastern Tibetan plateau since the middle Miocene. *Catena*, 208, 105785. <https://doi.org/10.1016/j.catena.2021.105785>
- Gehrels, G., Kapp, P., DeCelles, P., Pullen, A., Blakey, R., Weislogel, A., Ding, L., Guynn, J., Martin, A., McQuarrie, N., & Yin, A. (2011). Detrital zircon geochronology of pre-tertiary strata in the Tibetan-Himalayan orogen. *Tectonics*, 30, TC5016. <https://doi.org/10.1029/2011TC002868>
- Gehrels, G., Yin, A., & Wang, X. (2003a). Detrital-zircon geochronology of the northeastern Tibetan plateau. *Geological Society of*

- America Bulletin*, 115, 881–896. [https://doi.org/10.1130/0016-7606\(2003\)115<0881:DGOTNT>2.0.CO;2](https://doi.org/10.1130/0016-7606(2003)115<0881:DGOTNT>2.0.CO;2)
- Gehrels, G., Yin, A., & Wang, X. F. (2003b). Magmatic history of the northeastern Tibetan plateau. *Journal of Geophysical Research-Solid Earth*, 108, 1–14. <https://doi.org/10.1029/2002jb001876>
- George, A. D., Marshallsea, S. J., Wyrwoll, K. H., Jie, C., & Yanchou, L. (2001). Miocene cooling in the northern Qilian Shan, northeastern margin of the Tibetan plateau, revealed by apatite fission-track and vitrinite-reflectance analysis. *Geology*, 29(10), 939–942. [https://doi.org/10.1130/0091-7613\(2001\)029<0939:MCITNQ>2.0.CO;2](https://doi.org/10.1130/0091-7613(2001)029<0939:MCITNQ>2.0.CO;2)
- Gong, S., Chen, N., Wang, Q., Kusky, T. M., Wang, L., Zhang, L., Ba, J., & Liao, F. (2012). Early Paleoproterozoic magmatism in the Qianji massif, northeastern margin of the Qinghai-Tibet plateau and its tectonic significance: LA-ICPMS U-pb zircon geochronology and geochemistry. *Gondwana Research*, 21(1), 152–166. <https://doi.org/10.1016/j.gr.2011.07.011>
- Guan, P., & Jian, X. (2013). The Cenozoic sedimentary record in Qaidam basin and its implications for tectonic evolution of the northern Tibetan plateau. *Acta Sedimentologica Sinica*, 31, 824–833 (In Chinese with English abstract).
- Guo, P., Liu, C., Huang, L., Wang, P., Wang, K., Yuan, H., Xu, C., & Zhang, Y. (2017). Genesis of the late Eocene bedded halite in the Qaidam Basin and its implication for paleoclimate in East Asia. *Palaeogeography, Palaeoclimatology, Palaeoecology*, 487, 364–380. <https://doi.org/10.1016/j.palaeo.2017.09.023>
- Guo, Z. T., Sun, B., Zhang, Z. S., Peng, S. Z., Xiao, G. Q., Ge, J. Y., Hao, Q. Z., Qiao, Y. S., Liang, M. Y., Liu, J. F., Yin, Q. Z., & Wei, J. J. (2008). A major reorganization of Asian climate by the early Miocene. *Climate of the Past*, 4(3), 153–174. www.clim-past.net/4/153/2008/
- He, D., Dong, Y., Liu, X., Zhou, X., Zhang, F., & Sun, S. (2018). Zircon U–Pb geochronology and Hf isotope of granitoids in East Kunlun: Implications for the Neoproterozoic magmatism of Qaidam Block, Northern Tibetan Plateau. *Precambrian Research*, 314, 377–393. <https://doi.org/10.1016/j.precamres.2018.06.017>
- He, P., Song, C., Wang, Y., Wang, D., Chen, L., Meng, Q., & Fang, X. (2021). Early Cenozoic activated deformation in the Qilian Shan, northeastern Tibetan plateau: Insights from detrital apatite fission-track analysis. *Basin Research*, 33(3), 1731–1748. <https://doi.org/10.1111/bre.12533>
- Hong, D., Jian, X., Fu, L., & Zhang, W. (2020). Garnet trace element geochemistry as a sediment provenance indicator: An example from the Qaidam basin, northern Tibet. *Marine and Petroleum Geology*, 116, 104316. <https://doi.org/10.1016/j.marpetgeo.2020.104316>
- Horton, B. K., Dupont-Nivet, G., Zhou, J., Waanders, G. L., Butler, R. F., & Wang, J. (2004). Mesozoic-Cenozoic evolution of the Xining-Minhe and Dangchang basins, northeastern Tibetan plateau: Magnetostratigraphic and biostratigraphic results. *Journal of Geophysical Research: Solid Earth*, 109, B04402. <https://doi.org/10.1029/2003JB002913>
- Horton, B. K., Yin, A., Spurlin, M. S., Zhou, J. Y., & Wang, J. H. (2002). Paleocene-Eocene syncontractional sedimentation in narrow, lacustrine-dominated basins of east-Central Tibet. *Geological Society of America Bulletin*, 114, 771–786. [https://doi.org/10.1130/0016-7606\(2002\)114<0771:PESSIN>2.0.CO;2](https://doi.org/10.1130/0016-7606(2002)114<0771:PESSIN>2.0.CO;2)
- Hubert, J. F. (1962). A zircon-tourmaline-rutile maturity index and the interdependence of the composition of heavy mineral assemblages with the gross composition and texture of sandstones. *Journal of Sedimentary Petrology*, 32, 440–450. <https://doi.org/10.1306/74D70CE5-2B21-11D7-8648000102C1865D>
- Jackson, W. T., Jr., Robinson, D. M., Weislogel, A. L., & Jian, X. (2020). Cenozoic reactivation along the late Triassic Ganzi-Litang suture, eastern Tibetan plateau. *Geoscience Frontiers*, 11(3), 1069–1080. <https://doi.org/10.1016/j.gsf.2019.11.001>
- Jackson, W. T., Jr., Robinson, D. M., Weislogel, A. L., Jian, X., & McKay, M. P. (2018). Cenozoic development of the nonmarine Mula basin in the southern Yidun terrane: Deposition and deformation in the eastern Tibetan plateau associated with the India-Asia collision. *Tectonics*, 37(8), 2446–2465. <https://doi.org/10.1029/2018TC004994>
- Ji, J., Zhang, K., Clift, P. D., Zhuang, G., Song, B., Ke, X., & Xu, Y. (2017). High-resolution magnetostratigraphic study of the Paleogene-Neogene strata in the northern Qaidam Basin: Implications for the growth of the northeastern Tibetan plateau. *Gondwana Research*, 46, 141–155. <https://doi.org/10.1016/j.gr.2017.02.015>
- Jian, X., Guan, P., Fu, S.-T., Zhang, D.-W., Zhang, W., & Zhang, Y.-S. (2014). Miocene sedimentary environment and climate change in the northwestern Qaidam basin, northeastern Tibetan plateau: Facies, biomarker and stable isotopic evidences. *Palaeogeography, Palaeoclimatology, Palaeoecology*, 414, 320–331. <https://doi.org/10.1016/j.palaeo.2014.09.011>
- Jian, X., Guan, P., Zhang, D. W., Zhang, W., Feng, F., Liu, R. J., & Lin, S. D. (2013). Provenance of tertiary sandstone in the northern Qaidam basin, northeastern Tibetan plateau: Integration of framework petrography, heavy mineral analysis and mineral chemistry. *Sedimentary Geology*, 290, 109–125. <https://doi.org/10.1016/j.sedgeo.2013.03.010>
- Jian, X., Guan, P., Zhang, W., & Feng, F. (2013). Geochemistry of Mesozoic and Cenozoic sediments in the northern Qaidam basin, northeastern Tibetan plateau: Implications for provenance and weathering. *Chemical Geology*, 360, 74–88. <https://doi.org/10.1016/j.chemgeo.2013.10.011>
- Jian, X., Guan, P., Zhang, W., Liang, H., Feng, F., & Fu, L. (2018). Late cretaceous to early Eocene deformation in the northern Tibetan plateau: Detrital apatite fission track evidence from northern Qaidam basin. *Gondwana Research*, 60, 94–104. <https://doi.org/10.1016/j.gr.2018.04.007>
- Jian, X., Weislogel, A., & Pullen, A. (2019). Triassic sedimentary filling and closure of the eastern paleo-Tethys Ocean: New insights from detrital zircon geochronology of Songpan-Ganzi, Yidun, and west Qinling flysch in eastern Tibet. *Tectonics*, 38(2), 767–787. <https://doi.org/10.1029/2018TC005300>
- Jian, X., Weislogel, A., Pullen, A., & Shang, F. (2020). Formation and evolution of the eastern Kunlun range, northern Tibet: Evidence from detrital zircon U-pb geochronology and hf isotopes. *Gondwana Research*, 83, 63–79. <https://doi.org/10.1016/j.gr.2020.01.015>
- Jian, X., Zhang, W., Liang, H., Guan, P., & Fu, L. (2019). Mineralogy, petrography and geochemistry of an early Eocene weathering profile on basement granodiorite of Qaidam basin, northern Tibet: Tectonic and paleoclimatic implications. *Catena*, 172, 54–64. <https://doi.org/10.1016/j.catena.2018.07.029>
- Jian, X., Zhang, W., Yang, S., & Kao, S. J. (2020). Climate-dependent sediment composition and transport of mountainous rivers in tectonically stable, subtropical East Asia. *Geophysical Research Letters*, 47(3), e2019GL086150. <https://doi.org/10.1029/2019GL086150>

- Jin, C., Liu, Q., Liang, W., Roberts, A. P., Sun, J., Hu, P., Zhao, X., Su, Y., Jiang, Z., Liu, Z., Duan, Z., Yang, H., & Yuan, S. (2018). Magnetostratigraphy of the Fenghuoshan Group in the Hoh Xil Basin and its tectonic implications for India-Eurasia collision and Tibetan Plateau deformation. *Earth and Planetary Science Letters*, 486, 41–53. <https://doi.org/10.1016/j.epsl.2018.01.010>
- Kapp, P., DeCelles, P. G., Gehrels, G. E., Heizler, M., & Ding, L. (2007). Geological records of the Lhasa-Qiangtang and Indo-Asian collisions in the Nima area of Central Tibet. *Geological Society of America Bulletin*, 119, 917–933. <https://doi.org/10.1130/B26033.1>
- Kapp, P., Yin, A., Harrison, T. M., & Ding, L. (2005). Cretaceous-Tertiary shortening, basin development, and volcanism in central Tibet. *Geological Society of America Bulletin*, 117, 865–878. <https://doi.org/10.1130/B25595.1>
- Kong, X., Yin, A., & Harrison, T. M. (1997). Evaluating the role of preexisting weaknesses and topographic distributions in the Indo-Asian collision by use of a thin-shell numerical model. *Geology*, 25(6), 527–530. [https://doi.org/10.1130/0091-7613\(1997\)025<0527:ETROPW>2.3.CO;2](https://doi.org/10.1130/0091-7613(1997)025<0527:ETROPW>2.3.CO;2)
- Lease, R. O., Burbank, D. W., Gehrels, G. E., Wang, Z., & Yuan, D. (2007). Signatures of mountain building: Detrital zircon U/pb ages from northeastern Tibet. *Geology*, 35(3), 239–242. <https://doi.org/10.1130/G23057A.1>
- Li, B., Zuza, A. V., Chen, X., Hu, D., Shao, Z., Qi, B., Wang, Z., Levy, D. A., & Xiong, X. (2020). Cenozoic multi-phase deformation in the Qilian Shan and out-of-sequence development of the northern Tibetan plateau. *Tectonophysics*, 782, 228423. <https://doi.org/10.1016/j.tecto.2020.228423>
- Li, D., Chen, Y., Zhou, J., Kang, H., & Hou, K. (2020). Continuity of the Western Qinling and Qaidam-Qilian blocks: Evidence from Precambrian and Permian-Triassic strata around the Gonghe Basin area, NW China. *Geological Journal*, 55(5), 3601–3614. <https://doi.org/10.1002/gj.3610>
- Li, W., Neubauer, F., Liu, Y., Genser, J., Ren, S., Han, G., & Liang, C. (2013). Paleozoic evolution of the Qimantagh magmatic arcs, eastern Kunlun Mountains: Constraints from zircon dating of granitoids and modern river sands. *Journal of Asian Earth Sciences*, 77, 183–202. <https://doi.org/10.1016/j.jseaes.2013.08.030>
- Liang, Y., Zhang, B., Zhang, Y., Zhang, Y., Wang, J., & Liu, Z. (2021). Evolution of the Miocene megalake in the western Qaidam Basin, northwestern China. *Palaeogeography, Palaeoclimatology, Palaeoecology*, 571, 110384. <https://doi.org/10.1016/j.palaeo.2021.110384>
- Liu, Y., Neubauer, F., Li, W., Genser, J., & Li, W. (2012). Tectonothermal events of the northern Qaidam margin-southern Qilian area, western China. *Journal of Jilin University (Earth Science Edition)*, 42, 1317–1329 (In Chinese with English abstract).
- Lu, H., Ye, J., Guo, L., Pan, J., Xiong, S., & Li, H. (2018). Towards a clarification of the provenance of Cenozoic sediments in the northern Qaidam Basin. *Lithosphere*, 11(2), 252–272. <https://doi.org/10.1130/L1037.1>
- McRivette, M. W., Yin, A., Chen, X., & Gehrels, G. E. (2019). Cenozoic basin evolution of the central Tibetan plateau as constrained by U-pb detrital zircon geochronology, sandstone petrology, and fission-track thermochronology. *Tectonophysics*, 751, 150–179. <https://doi.org/10.1016/j.tecto.2018.12.015>
- Meijer, N., Dupont-Nivet, G., Abels, H. A., Kaya, M. Y., Licht, A., Xiao, M., Zhang, Y., Roperch, P., Poujol, M., Lai, Z., & Guo, Z. (2019). Central Asian moisture modulated by proto-Paratethys Sea incursions since the early Eocene. *Earth and Planetary Science Letters*, 510, 73–84. <https://doi.org/10.1016/j.epsl.2018.12.031>
- Miao, Y., Herrmann, M., Wu, F., Yan, X., & Yang, S. (2012). What controlled Mid-Late Miocene long-term aridification in Central Asia?—Global cooling or Tibetan Plateau uplift: A review. *Earth-Science Reviews*, 112(3–4), 155–172. <https://doi.org/10.1016/j.earscirev.2012.02.003>
- Molnar, P., Boos, W. R., & Battisti, D. S. (2010). Orographic controls on climate and paleoclimate of Asia: Thermal and mechanical roles for the Tibetan plateau. *Annual Review of Earth and Planetary Sciences*, 38, 77–102. <https://doi.org/10.1146/annurev-earth-040809-152456>
- Molnar, P., England, P., & Martinod, J. (1993). Mantle dynamics, uplift of the Tibetan plateau, and the Indian monsoon. *Reviews of Geophysics*, 31, 357–396. <https://doi.org/10.1029/93RG02030>
- Molnar, P., & Stock, J. M. (2009). Slowing of India's convergence with Eurasia since 20 Ma and its implications for Tibetan mantle dynamics. *Tectonics*, 28, TC3001. <https://doi.org/10.1029/2008TC002271>
- Morton, A. C., & Hallsworth, C. R. (1994). Identifying provenance-specific features of detrital heavy mineral assemblages in sandstones. *Sedimentary Geology*, 90, 241–256. [https://doi.org/10.1016/0037-0738\(94\)90041-8](https://doi.org/10.1016/0037-0738(94)90041-8)
- Murphy, M. A., Yin, A., Harrison, T. M., Dürr, S. B., Chen, Z., Ryerson, F. J., Kidd, W. S. F., Wang, X., & Zhou, X. (1997). Did the Indo-Asian collision alone create the Tibetan plateau? *Geology*, 25, 719–722. [https://doi.org/10.1130/0091-7613\(1997\)025<0719:DTIACA>2.3.CO;2](https://doi.org/10.1130/0091-7613(1997)025<0719:DTIACA>2.3.CO;2)
- Najman, Y., Appel, E., Boudagher-Fadel, M., Bown, P., Carter, A., Garzanti, E., Godin, L., Han, J., Liebke, U., Oliver, G., Parrish, R., & Vezzoli, G. (2010). Timing of India-Asia collision: Geological, biostratigraphic, and palaeomagnetic constraints. *Journal of Geophysical Research-Solid Earth*, 115, B12416. <https://doi.org/10.1029/2010JB007673>
- Nie, J., Ren, X., Saylor, J. E., Su, Q., Horton, B. K., Bush, M. A., Chen, W., & Pfaff, K. (2020). Magnetic polarity stratigraphy, provenance, and paleoclimate analysis of Cenozoic strata in the Qaidam Basin, NE Tibetan Plateau. *GSA Bulletin*, 132(1–2), 310–320. <https://doi.org/10.1130/B35175.1>
- Raymo, M. E., & Ruddiman, W. F. (1992). Tectonic forcing of late Cenozoic climate. *Nature*, 359, 117–122.
- Rieser, A. B., Neubauer, F., Liu, Y., & Ge, X. (2005). Sandstone provenance of north-western sectors of the intracontinental Cenozoic Qaidam basin, western China: Tectonic vs. climatic control. *Sedimentary Geology*, 177(1–2), 1–18. <https://doi.org/10.1016/j.sedgeo.2005.01.012>
- Rohrmann, A., Kapp, P., Carrapa, B., Reiners, P. W., Guynn, J., Ding, L., & Heizler, M. (2012). Thermochronologic evidence for plateau formation in Central Tibet by 45 Ma. *Geology*, 40, 187–190. <https://doi.org/10.1130/G32530.1>
- Song, B., Zhang, K., Hou, Y., Ji, J., Wang, J., Yang, Y., Yang, T., Wang, C., & Shen, T. (2019). New insights into the provenance of Cenozoic strata in the Qaidam Basin, northern Tibet: Constraints from combined U-pb dating of detrital zircons in recent and ancient fluvial sediments. *Palaeogeography, Palaeoclimatology, Palaeoecology*, 533, 109254. <https://doi.org/10.1016/j.palaeo.2019.109254>
- Song, S. G., Su, L., Li, X. H., Niu, Y. L., & Zhang, L. F. (2012). Grenville orogenesis in the Qaidam-Qilian block: The link between

- South China and Tarim. *Precambrian Research*, 220–221, 9–22. <https://doi.org/10.1016/j.precamres.2012.07.007>
- Spurlin, M. S., Yin, A., Horton, B. K., Zhou, J., & Wang, J. (2005). Structural evolution of the Yushu-Nangqian region and its relationship to syncollisional igneous activity east-Central Tibet. *Geological Society of America Bulletin*, 117, 1293–1317. <https://doi.org/10.1130/B25572.1>
- Studnicki-Gizbert, C., Burchfiel, B. C., Li, Z., & Chen, Z. (2008). Early tertiary Gonjo basin, eastern Tibet: Sedimentary and structural record of the early history of India-Asia collision. *Geosphere*, 4, 713–735. <https://doi.org/10.1130/GES00136.1>
- Sun, Y., Liu, J., Liang, Y., Ji, J., Liu, W., Aitchison, J. C., Sun, J., Lu, J., Song, B., Xu, Y., Zhang, K., & Liu, Z. (2020). Cenozoic moisture fluctuations on the northeastern Tibetan plateau and association with global climatic conditions. *Journal of Asian Earth Sciences*, 200, 104490. <https://doi.org/10.1016/j.jseas.2020.104490>
- Sun, Z., Yang, Z., Pei, J., Ge, X., Wang, X., Yang, T., Li, W., & Yuan, S. (2005). Magnetostratigraphy of Paleogene sediments from northern Qaidam Basin, China: Implications for tectonic uplift and block rotation in northern Tibetan plateau. *Earth and Planetary Science Letters*, 237(3–4), 635–646. <https://doi.org/10.1016/j.epsl.2005.07.007>
- Tang, M., Liu-Zeng, J., Hoke, G. D., Xu, Q., Wang, W., Li, Z., Zhang, J., & Wang, W. (2017). Paleoelevation reconstruction of the Paleocene-Eocene Gonjo basin, SE-Central Tibet. *Tectonophysics*, 712–713, 170–181. <https://doi.org/10.1016/j.tecto.2017.05.018>
- Tapponnier, P., Xu, Z., Roger, F., Meyer, B., Arnaud, N., Wittlinger, G., & Yang, J. (2001). Oblique stepwise rise and growth of the Tibet plateau. *Science*, 294, 1671–1677. <https://doi.org/10.1126/science.105978>
- Van Hinsbergen, D. J., Lippert, P. C., Dupont-Nivet, G., McQuarrie, N., Doubrovine, P. V., Spakman, W., & Torsvik, T. H. (2012). Greater India Basin hypothesis and a two-stage Cenozoic collision between India and Asia. *Proceedings of the National Academy of Sciences*, 109, 7659–7664. <https://doi.org/10.1073/pnas.1117262109>
- Vermeesch, P. (2012). On the visualization of detrital age distributions. *Chemical Geology*, 312–313, 190–194. <https://doi.org/10.1016/j.chemgeo.2012.04.021>
- Vermeesch, P., Resentini, A., & Garzanti, E. (2016). An R package for statistical provenance analysis. *Sedimentary Geology*, 336, 14–25. <https://doi.org/10.1016/j.sedgeo.2016.01.009>
- Volkmer, J. E., Kapp, P., Guynn, J. H., & Lai, Q. (2007). Cretaceous-tertiary structural evolution of the north Central Lhasa terrane, Tibet. *Tectonics*, 26, TC6007. <https://doi.org/10.1029/2005TC001832>
- Wang, C., Dai, J., Zhao, X., Li, Y., Graham, S. A., He, D., Ran, B., & Meng, J. (2014). Outward-growth of the Tibetan plateau during the Cenozoic: A review. *Tectonophysics*, 621, 1–43. <https://doi.org/10.1016/j.tecto.2014.01.036>
- Wang, C., Zhao, X., Liu, Z., Lippert, P. C., Graham, S. A., Coe, R. S., Yi, H., Zhu, L., Liu, S., & Li, Y. (2008). Constraints on the early uplift history of the Tibetan plateau. *Proceedings of the National Academy of Sciences*, 105, 4987–4992. <https://doi.org/10.1073/pnas.0703595105>
- Wang, Q., Chen, N., Li, X., Hao, S., & Chen, H. (2008). LA-ICPMS zircon U-pb geochronological constraints on the tectonothermal evolution of the early Paleoproterozoic Dakendaban Group in the Quanji Block, NW China. *Chinese Science Bulletin*, 53, 2849–2858. <https://doi.org/10.1007/s11434-008-0265-x>
- Wang, W., Zheng, W., Zhang, P., Li, Q., Kirby, E., Yuan, D., Zheng, D., Liu, C., Wang, Z., Zhang, H., & Pang, J. (2017). Expansion of the Tibetan plateau during the Neogene. *Nature Communications*, 8, 15887. <https://doi.org/10.1038/ncomms15887>
- Wang, Y., Zheng, J., Zheng, Y., Liu, X., & Sun, G. (2015). Paleocene-early Eocene uplift of the Altyn Tagh Mountain: Evidence from detrital zircon fission track analysis and seismic sections in the northwestern Qaidam basin. *Journal of Geophysical Research: Solid Earth*, 120(12), 8534–8550. <https://doi.org/10.1002/2015JB011922>
- Wu, C., Yin, A., Zuza, A. V., Zhang, J., Liu, W., & Ding, L. (2016). Pre-Cenozoic geologic history of the central and northern Tibetan plateau and the role of Wilson cycles in constructing the Tethyan orogenic system. *Lithosphere*, 8(3), 254–292. <https://doi.org/10.1130/L494.1>
- Wu, C., Zuza, A. V., Zhou, Z., Yin, A., McRivette, M. W., Chen, X., Ding, L., & Geng, J. (2019). Mesozoic-Cenozoic evolution of the eastern Kunlun range, Central Tibet, and implications for basin evolution during the Indo-Asian collision. *Lithosphere*, 11, 524–550. <https://doi.org/10.1130/L1065.1>
- Wu, L., Lin, X., Cowgill, E., Xiao, A., Cheng, X., Chen, H., Zhao, H., Shen, Y., & Yang, S. (2019). Middle Miocene reorganization of the Altyn Tagh fault system, northern Tibetan plateau. *GSA Bulletin*, 131(7–8), 1157–1178. <https://doi.org/10.1130/B31875.1>
- Wu, M., Zhuang, G., Hou, M., & Liu, Z. (2021). Expanded lacustrine sedimentation in the Qaidam Basin on the northern Tibetan plateau: Manifestation of climatic wetting during the Oligocene icehouse. *Earth and Planetary Science Letters*, 565, 116935. <https://doi.org/10.1016/j.epsl.2021.116935>
- Xie, X., & Heller, P. L. (2013). U–Pb detrital zircon geochronology and its implications: The early Late Triassic Yanchang Formation, south Ordos Basin, China. *Journal of Asian Earth Sciences*, 64, 86–98. <https://doi.org/10.1016/j.jseas.2012.11.045>
- Xu, W. C., Zhang, H. F., & Liu, X. M. (2007). U-pb zircon dating constraints on formation time of Qilian high-grade metamorphic rock and its tectonic implications. *Chinese Science Bulletin*, 52, 531–538. <https://doi.org/10.1007/s11434-007-0082-7>
- Yin, A., Dang, Y., Wang, L., Jiang, W., Zhou, S., Chen, X., Gehrels, G. E., & McRivette, M. W. (2008). Cenozoic tectonic evolution of Qaidam basin and its surrounding regions (part 1): The southern Qilian Shan-Nan Shan thrust belt and northern Qaidam basin. *Geological Society of America Bulletin*, 120, 813–846. <https://doi.org/10.1130/B26180.1>
- Yin, A., Dang, Y., Zhang, M., Chen, X., & McRivette, M. W. (2008). Cenozoic tectonic evolution of the Qaidam basin and its surrounding regions (part 3): Structural geology, sedimentation, and regional tectonic reconstruction. *Geological Society of America Bulletin*, 120(12), 847–876. <https://doi.org/10.1130/B26232.1>
- Yin, A., & Harrison, T. M. (2000). Geologic evolution of the Himalayan-Tibetan orogen. *Annual Review of Earth and Planetary Sciences*, 28, 211–280. <https://doi.org/10.1146/annurev.earth.28.1.211>
- Yu, S. Y., Zhang, J. X., del Real, P. G., Zhao, X. L., Hou, K. J., Gong, J. G., & Li, Y. S. (2013). The Grenvillian orogeny in the Altyn-Qilian-north Qaidam mountain belts of northern Tibet plateau: Constraints from geochemical and zircon

- U-pb age and hf isotopic study of magmatic rocks. *Journal of Asian Earth Sciences*, 73, 372–395. <https://doi.org/10.1016/j.jseas.2013.04.042>
- Yu, X., Fu, S., Wang, Z., Li, Q., & Guo, Z. (2017). The discovery of early Paleoproterozoic high-Na trondhjemite in the northeastern Qaidam basin: Evidence from the drilling core samples. *Precambrian Research*, 298, 615–628. <https://doi.org/10.1016/j.precamres.2017.04.002>
- Yu, X., Guo, Z., Du, W., & Wang, Z. (2021). Coupling between surface processes and crustal deformation: Insights from the late Cenozoic development of the Qaidam Basin, China. *Global and Planetary Change*, 207, 103646. <https://doi.org/10.1016/j.gloplacha.2021.103646>
- Yu, X., Guo, Z., Guan, S., Du, W., Wang, Z., Bian, Q., & Li, L. (2019). Landscape and tectonic evolution of Bayin River watershed, northeastern Qaidam basin, northern Tibetan plateau: Implications for the role of river morphology in source analysis and low-temperature thermochronology. *Journal of Geophysical Research: Earth Surface*, 124(7), 1701–1719. <https://doi.org/10.1029/2018JF004989>
- Yu, X., Guo, Z., Zhang, Q., Cheng, X., Du, W., Wang, Z., & Bian, Q. (2017). Denan depression controlled by northeast-directed Olongbulak thrust zone in northeastern Qaidam basin: Implications for growth of northern Tibetan plateau. *Tectonophysics*, 717, 116–126. <https://doi.org/10.1016/j.tecto.2017.06.017>
- Yuan, D.-Y., Ge, W.-P., Chen, Z.-W., Li, C.-Y., Wang, Z.-C., Zhang, H.-P., Zhang, P.-Z., Zheng, D.-W., Zheng, W.-J., Craddock, W. H., Dayem, K. E., Duvall, A. R., Hough, B. G., Lease, R. O., Champagnac, J.-D., Burbank, D. W., Clark, M. K., Farley, K. A., Garzzone, C. N., ... Roe, G. H. (2013). The growth of northeastern Tibet and its relevance to large-scale continental geodynamics: A review of recent studies. *Tectonics*, 32, 1358–1370. <https://doi.org/10.1002/tect.20081>
- Zeng, X., Tian, J., Zhang, G., Zhao, J., Wu, P., & Wang, W. (2018). Main types and hydrocarbon exploration direction of the paleo-uplifts in the Qaidam basin. *Journal of Geomechanics*, 24(3), 381–390 (In Chinese with English abstract).
- Zhang, P. Z., Shen, Z., Wang, M., Gan, W., Bürgmann, R., Molnar, P., Wang, Q., Niu, Z., Sun, J., Wu, J., Hanrong, S., & Xinzhaoy, Y. (2004). Continuous deformation of the Tibetan plateau from global positioning system data. *Geology*, 32(9), 809–812. <https://doi.org/10.1130/G20554.1>
- Zhang, S., Jian, X., Pullen, A., Fu, L., Liang, H., Hong, D., & Zhang, W. (2021). Tectono-magmatic events of the Qilian orogenic belt in northern Tibet: New insights from detrital zircon geochronology of river sands. *International Geology Review*, 63(8), 917–940. <https://doi.org/10.1080/00206814.2020.1734876>
- Zhang, W., Jian, X., Fu, L., Feng, F., & Guan, P. (2018). Reservoir characterization and hydrocarbon accumulation in late Cenozoic lacustrine mixed carbonate-siliciclastic fine-grained deposits of the northwestern Qaidam basin, NW China. *Marine and Petroleum Geology*, 98, 675–686. <https://doi.org/10.1016/j.marpetgeo.2018.09.008>
- Zhang, Y. P., Zheng, W. J., Wang, W. T., Tian, Y. T., Zhou, R., Xu, B. B., Li, M. J., Yan, Y. G., Tian, Q. Y., & Zhang, P. Z. (2020). Rapid Eocene exhumation of the west Qinling Belt: Implications for the growth of the northeastern Tibetan plateau. *Lithosphere*, 2020(1), 8294751. <https://doi.org/10.2113/2020/8294751>
- Zheng, D., Clark, M. K., Zhang, P., Zheng, W., & Farley, K. A. (2010). Erosion, fault initiation and topographic growth of the north Qilian Shan (northern Tibetan plateau). *Geosphere*, 6(6), 937–941. <https://doi.org/10.1130/GES00523.1>
- Zhu, W., Wu, C., Wang, J., Zhou, T., Li, J., Zhang, C., & Li, L. (2017). Heavy mineral compositions and zircon U-pb ages of Cenozoic sandstones in the SW Qaidam basin, northern Tibetan plateau: Implications for provenance and tectonic setting. *Journal of Asian Earth Sciences*, 146, 233–250. <https://doi.org/10.1016/j.jseas.2017.05.023>
- Zhuang, G., Hourigan, J. K., Ritts, B. D., & Kent-Corson, M. L. (2011). Cenozoic multiple-phase tectonic evolution of the northern Tibetan plateau: Constraints from sedimentary records from Qaidam basin, Hexi corridor, and Subei basin, Northwest China. *American Journal of Science*, 311, 116–152. <https://doi.org/10.2475/02.2011.02>
- Zhuang, G., Johnstone, S. A., Hourigan, J., Ritts, B., Robinson, A., & Sobel, E. R. (2018). Understanding the geologic evolution of northern Tibetan plateau with multiple thermochronometers. *Gondwana Research*, 58, 195–210. <https://doi.org/10.1016/j.gr.2018.02.014>
- Zuza, A. V., Cheng, X., & Yin, A. (2016). Testing models of Tibetan plateau formation with Cenozoic shortening estimates across the Qilian Shan-Nan Shan thrust belt. *Geosphere*, 12(2), 501–532. <https://doi.org/10.1130/GES01254.1>
- Zuza, A. V., Wu, C., Reith, R. C., Yin, A., Li, J., Zhang, J., Zhang, Y., Wu, L., & Liu, W. (2018). Tectonic evolution of the Qilian Shan: An early Paleozoic orogen reactivated in the Cenozoic. *GSA Bulletin*, 130, 881–925. <https://doi.org/10.1130/B31721.1>
- Zuza, A. V., Wu, C., Wang, Z., Levy, D. A., Li, B., Xiong, X., & Chen, X. (2019). Underthrusting and duplexing beneath the northern Tibetan plateau and the evolution of the Himalayan-Tibetan orogen. *Lithosphere*, 11(2), 209–231. <https://doi.org/10.1130/L1042.1>

SUPPORTING INFORMATION

Additional supporting information can be found online in the Supporting Information section at the end of this article.

How to cite this article: Jian, X., Fu, L., Wang, P., Guan, P., Zhang, W., Fu, H., & Mei, H. (2023). Sediment provenance of the Lulehe Formation in the Qaidam basin: Insight to initial Cenozoic deposition and deformation in northern Tibetan plateau. *Basin Research*, 35, 271–294. <https://doi.org/10.1111/bre.12712>